Chapter 12
Aerosols in Titan's Atmosphere

Martin G. Tomasko and Robert A. West

Abstract Aerosols in Titan's atmosphere play important roles in the transfer of solar and thermal radiation, in Titan's heat balance, in forcing atmospheric dynamics, and as a sink for photochemical reactions. In this chapter we briefly summarize the history of our knowledge of their distribution and optical properties before concentrating in greater detail on current knowledge of their properties and roles in the physics and chemistry in Titan's atmosphere. We discuss the size, shape, optical properties, and the vertical distribution of Titan's aerosols. We discuss variations of the optical properties of the aerosols with wavelength, variations of the distribution of the aerosols over the disk of Titan, and the seasonal and long-term variations in structure. We discuss the visible and thermal opacity of the aerosols, and their roles in Titan's heat balance. We summarize the history and current state of laboratory simulations of these particles, and present our understanding of their formation and life cycles in one and two-dimensional microphysical models. We also discuss the presence, location, and variations in condensation clouds over Titan's disk. Finally, we indicate the prospects for further progress in understanding the origin, distribution, and properties of Titan's aerosols in the future.

12.1 Introduction

The presence of aerosols in Titan's atmosphere has been known since Titan's albedo spectrum was measured, and the shape of the spectrum provided the first clues to the nature of these particles. The deep methane bands at red and infrared (IR)

wavelengths require several km-amagats of methane gas for their formation (Trafton 1973). Titan's geometric albedo at blue and near ultraviolet (UV) wavelengths is lower than it would be due to molecular scattering from this abundance of clean gas. Absorbing aerosols located above most of the gaseous atmosphere are required to account for Titan's low geometric albedo at short wavelengths. The strong signatures of the methane absorption bands at red and longer wavelengths imply that the optical depths of the aerosols decrease rapidly with increasing wavelength, providing constraints on the size of the aerosol particles (Podolak and Danielson 1977).

Several significant advances in understanding the properties of Titan's aerosols occurred before the Cassini–Huygens mission. The flyby of Pioneer 11 in 1980 provided measurements of the linear polarization of blue and red sunlight scattered from Titan's disk at 90° scattering angle (Tomasko and Smith 1982). Similar measurements at other wavelengths soon followed from Voyager 2 (West et al. 1983). The degrees of polarization observed at scattering angles near 90° were very large, confirming the small size of the aerosols already deduced from their rapid decrease in opacity with increasing wavelength. However, the observations by Voyager at very high phase angles (Rages et al. 1983) showed that the aerosols produced strong forward scattering in addition to high linear polarization near 90° scattering angle. Spherical particles could not reproduce these two types of observations for the same particle size distribution, and workers concluded the aerosols in Titan's atmosphere were not spherical.

This situation led West (1991) to compute single scattering phase functions, degrees of polarization, and cross sections from large fractal aggregates of small, approximately spherical "monomers". These calculations showed that for loose aggregate structures the size of each monomer could be sufficiently small to produce the strong linear polarization while the larger size of the entire aggregate could provide the strong forward scattering. West and Smith (1991) showed that such particles had great promise for explaining these two different types of Titan observations. The size of the entire aggregate particles could still be sufficiently small to give the required rapid decrease in opacity with increasing wavelength to produce the strong methane bands at red and

M.G. Tomasko (✉)
Lunar and Planetary Laboratory, University of Arizona, Tucson, AZ, 85721, USA
e-mail: mtomasko@lpl.arizona.edu

R.A. West
Jet Propulsion Laboratory, California Institute of Technology, 4800 Oak Grove Drive, Pasadena, CA 91109, USA

R. Brown et al. (eds.), Titan from Cassini-Huygens,

infrared wavelengths while nearly explaining the low geometric albedo at blue and near ultraviolet wavelengths.

At wavelengths of 200 nm, the aggregates are sufficiently large compared to the wavelength that the single-scattering albedo is >0.5 for any imaginary refractive index. This is too large to reproduce the small geometric albedo of Titan in the ultraviolet. Courtin et al. (1991) discussed observations of the low ultraviolet geometric albedo of Titan, and concluded that a bimodal distribution including particles with radii not greater than 0.02 μm mixed with larger particles with radii in the range of 0.1 to 0.5 μm could fit the low UV albedo as well as the methane bands in red and near infrared wavelengths. This model did not explicitly include fractal aggregates; however, the model suggests that high altitude regions dominated by monomers alone above larger aggregate particles at lower altitudes might be capable of fitting the observed variation of geometric albedo with wavelength from the UV to the infrared. Rannou et al. (1997) used Voyager observations to constrain the altitude of production and the vertical profile of the particles near the region of formation. The Voyager images of separated layers at the limb of Titan indicated the complexity of this formation region.

The decrease of Titan's geometric albedo toward blue wavelengths is partly due to the increased opacity of the aerosols toward shorter wavelengths, but it also requires that the imaginary refractive index increase toward shorter wavelengths as well. Some estimates of the variation of refractive index as well as chemical identity were provided by early attempts to produce aerosol material in the laboratory. Khare et al. (1984) produced aerosol material which they termed "tholin" from mixtures of methane and nitrogen using an electric spark, and they published the refractive index of the solid brown or orange material produced in their reaction vessels. Many modelers used their values of imaginary index as a function of wavelength or small variations from it to produce models of Titan's geometric albedo spectrum that fit the planetary observations quite well. Chemical analyses of the composition of the tholins showed a complex mixture of a great many hydrocarbons.

Titan's aerosols play important roles in many physical and chemical processes in Titan's atmosphere. The low albedos of the aerosols at blue and shorter wavelengths absorb sunlight and heat the atmosphere at high altitudes. At longer wavelengths, the aerosols become optically thinner and permit thermal infrared radiation to escape to space. In this way they have been termed to act as an "anti-greenhouse" agent (McKay et al. 1989). Their roles in absorbing and scattering solar and thermal infrared radiation give them a strong role in the heat balance of Titan and in providing the forcing for atmospheric dynamics. In addition, their formation at high altitudes where ultraviolet sunlight penetrates implies that aerosol production provides a sink for products of methane photochemistry that contain large C to H ratios. Because of their important roles in these physical and chemical processes, gaining a greater understanding of the vertical and horizontal distribution, size, shape, and composition of Titan's aerosols were major goals of the Cassini–Huygens mission.

We present and discuss the new information about Titan's aerosols in this chapter. Sections 12.2–12.4 discuss the details of aerosol size and shape, vertical distribution, and variations of optical properties with wavelength. We present variations in properties over the disk and with time in Sections 12.5 and 12.6. We discuss the roles of the aerosols in Titan's heat balance and their microphysics in Sections 12.7 and 12.8. We outline some recent laboratory simulation studies in Section 12.9 and summarize some measurements of condensation clouds in Section 12.10. A final section discusses prospects for future progress on determining the nature of Titan's aerosols, including continued Cassini and Hubble Space Telescope observations as well as possible investigations on future missions.

12.2 Aerosol Size and Shape Estimates

Constraints on the size and shape of Titan's aggregate haze particles are available from the Descent Imager/Spectral Radiometer (DISR) observations as the Huygens probe descended through the Titan atmosphere (Tomasko et al. 2008a). The DISR instrument (Tomasko et al. 2002) measured the degree of linear polarization in two passbands centered at 938 nm ("red") and 491 nm ("blue") using crossed polarizing analyzers. For small aerosols, the position angle of linearly polarized light is known to be perpendicular to the scattering plane, so the measurements made through two orthogonal analyzers suffice to measure the total intensity and the degree of linear polarization. The linear polarization of the multiply scattered sunlight headed downward at a scattering angle of 90° was 0.65 in the red channel and 0.5 in the blue channel at the beginning of the measurements near 140 km altitude. In order to produce these high degrees of linear polarization in multiply scattered light, the degree of polarization produced in single scattering must be nearly 100%. Comparisons with model calculations constrained the radii of the monomers (which determine the minimum dimensions of the aggregate particles) to be near 0.05 μm as shown in Fig. 12.1.

The DISR instrument also measured the forward scattering nature of Titan's atmospheric aerosols using an upward-looking camera with a field of view from 20° to 70° from the zenith and covering 6° in azimuth. Some images were obtained within 10° from the azimuth of the sun. The isophote contours in these images were compared with models computed with various numbers of monomers of the size necessary to reproduce the observed linear polarization measurements. The DISR observations (see Fig. 12.2) required that the

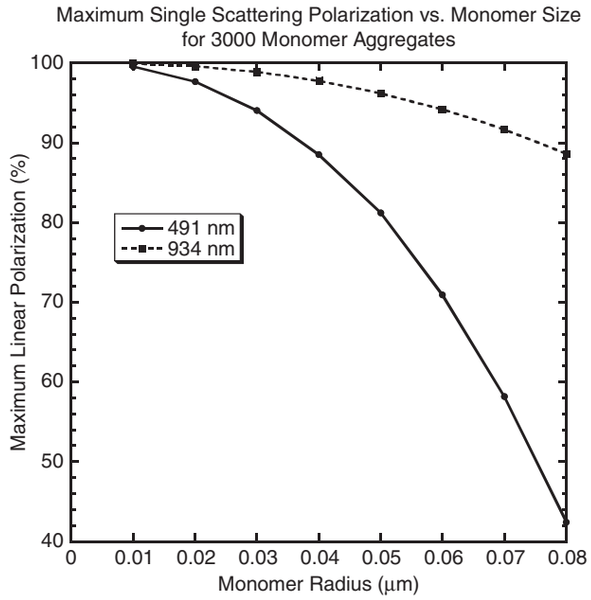

Fig. 12.1 The maximum degree of linear polarization in single scattering as a function of monomer radius at the wavelengths of the solar aureole channels of the DISR instrument is shown. In order to produce polarization of 60% in the red channel and 50% in the blue channel, Tomasko et al. (2008a) estimated that the monomer radius had to be approximately 0.05 μm or less. New models (Tomasko et al. 2009) of the DISR measurements indicate that the monomer radius is 0.04 μm

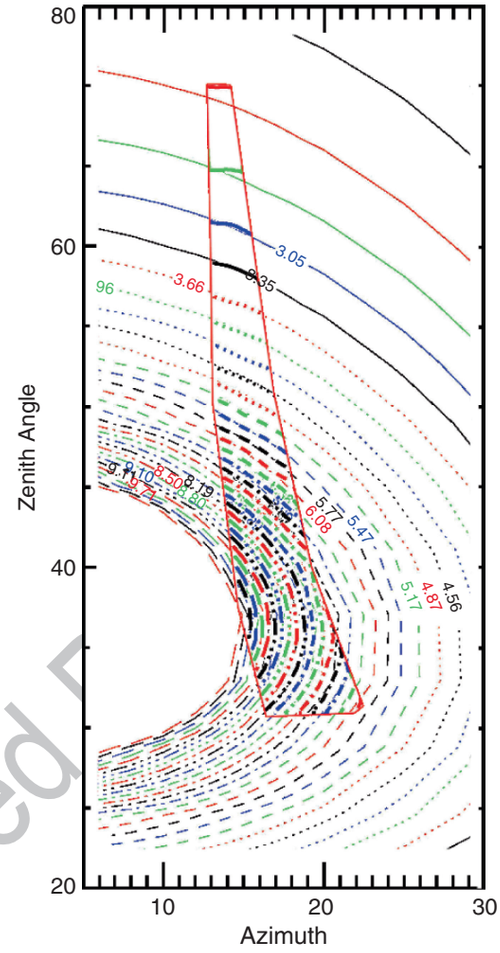

Fig. 12.2 The isophotes of intensity in the red solar aureole channel measured by the DISR instrument near the sun as measured near 60 km altitude are shown inside the red outline. The measured isophotes are compared to those of a model having 3,000 monomers of radius 0.05 μm. The model and the measurements are in good agreement

number of monomers in an aggregate haze particle when looking upward from 60 km altitude be about 3,000 (within a factor of ~2). This seemed to be much larger than the number of monomers used in some of the earlier work with aggregate particles, but still corresponds to only about a dozen collisions between clusters of similar size found between the altitude where the aerosols are formed and the 60 km altitude where the DISR measurements were made. The radius of a spherical particle with the same volume as the 3,000 monomers in the aggregate is 0.72 μm whereas the radius of a spherical particle with the same projected area as the aggregate particle is 2.03 μm. The forward scattering nature of the haze particles is shown in Fig. 12.3 where phase functions are given for different numbers of monomers in the aggregate particles.

More complete investigations of the DISR polarization measurements suggest that the monomer size changes only very little throughout the altitude range of the DISR measurements (between 140 km and the surface). The authors assumed that the forward part of the single scattering phase functions of the aerosols remained reasonably constant in this altitude range.

It should be emphasized that computation of the single scattering properties of aggregates with such a large number of monomers is a large computational challenge. In practice, computations are made for various particles with monomer numbers up to a few hundred, and extrapolations are made to still larger particles. The approximate technique used by Tomasko et al. (2008a) used in the analysis of the DISR observations is described in an appendix to their paper.

The wavelength dependence of the cross section of the aerosols can also constrain the size of the aerosol particles. The DISR investigators fit the wavelength dependence of the aerosol extinction with power laws in three separate altitude intervals, as shown in Fig. 12.4. Notice that the slope of the power law decreases with decreasing altitude, from −2.34 above 80 km, −1.41 between 80 and 30 km altitude, to −0.97 below 30 km. Steeper extinction power laws are associated with smaller particles, e. g. slopes may reach down to −4.0 for light scattering by particles very small compared to the wavelength (Rayleigh scattering). Flatter power laws are associated with larger particles, down to zero for particles very large compared to the wavelength. Note that the extraction

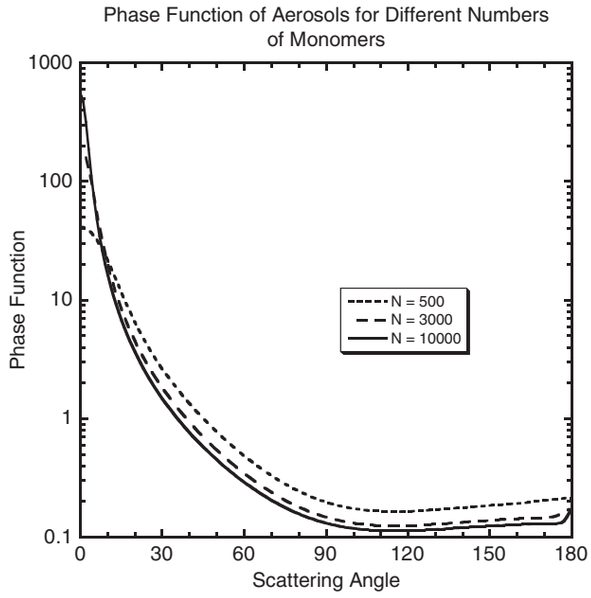

Fig. 12.3 The phase functions for aggregate particles grown by cluster-cluster collisions are shown for N different numbers of monomers each having a radius of 0.05 μm. The computations are for a wavelength of 934 nm (in the red channel of the DISR solar aureole camera)

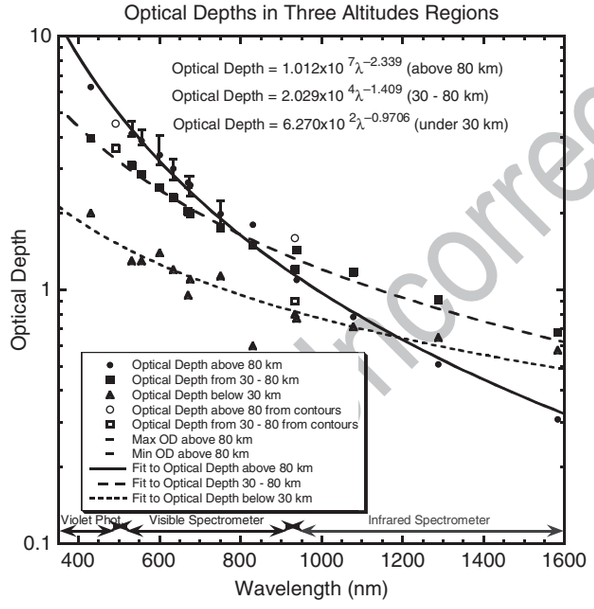

Fig. 12.4 The variation of extinction optical depth of the haze as functions of wavelength are shown for the haze particles above 80 km altitude, between 80 and 30 km altitude, and below 30 km as described by Tomasko et al. (2008a). The constraints imposed by the measurements are shown by points and are compared to power law fits shown by the lines. The slope of the variation with wavelength decreases with increasing depth into the atmosphere due to an increase in the size of the haze particles with decreasing altitude

of particle size depends on the accuracy with which the cross section for aggregate particles can be estimated for different sized aggregates. At altitudes greater than 80 km above

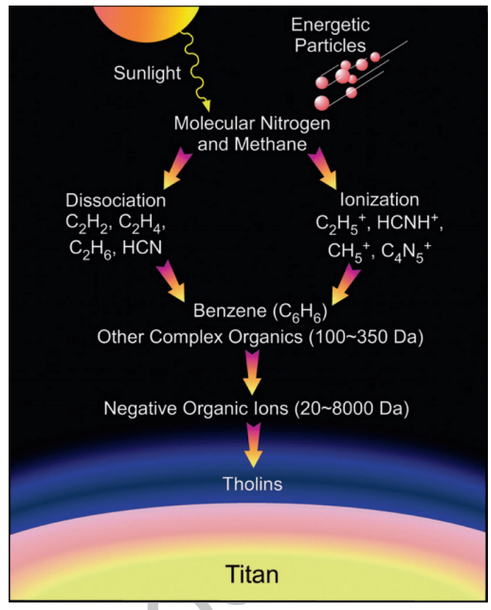

Fig. 12.5 Schematic diagram from Waite et al. (2007) showing the chemical processes leading up to the formation of tholins in Titan's upper atmosphere

Titan's surface, the DISR investigators reported that the variation of cross section from blue to red matched the estimates they used for loose fractal aggregates rather well. From 80 to 30 km above Titan's surface, the observed variations in aerosol cross section between blue and red matched less well, though still to within about a factor of two. Below 30 km the variations with wavelength were rather gentile, and could be fitted with particles large compared to the wavelength.

12.3 Vertical Distribution of Aerosols

The prevailing view of tholin haze formation emphasized the role of photochemical reactions in the stratosphere above about 100 km altitude (Yung et al. 1984; Wilson and Atreya 2003; Liang et al. 2007). Recent results from instruments on the Cassini orbiter call attention to ion and neutral chemistry in the high atmosphere, around 1,000 km altitude. A detailed discussion of atmospheric chemistry can be found elsewhere in this book (XX chapters on stratosphere and thermosphere chemistry). Here we highlight new findings which have bearing on aerosol formation as illustrated in Fig. 12.5.

Both the Ion and Neutral Mass Spectrometer (INMS) and the Ion Beam Spectrometer (IBS) on the Cassini Plasma Spectrometer (CAPS) instrument (Young et al. 2004) detected large molecules at altitudes above 950 km in Titan's thermosphere. This section summarizes findings presented by both instruments as reported by Waite et al. 2007. Mass spectra recorded by INMS show mass peaks that extend to the mass limit of the instrument. Of particular interest is the benzene

peak (C_6H_6) near 78 Da. Benzene is the smallest of the class of polycyclic aromatic hydrocarbons (PAHs) which are thought to be important for aerosol formation and are present in molecular clouds. The IBS measured positive and negative ions with charge/mass ratios up to the limit of its sensitivity near 10,000, although the number density falls rapidly above 4,000 Da.

The abundance of large negative ions was not anticipated but in retrospect seems understandable because of the electron affinities expected for PAHs and cyanoaromatics in the gas/plasma environment near the top of Titan's atmosphere. The actual mass of these clusters or proto-particles could be larger than several thousand Dalton if the charge per particle is greater than 1. Waite et al. (personal communication 2008) estimate effective radii of these large ions in the range 7.5–26 nm. These values are a factor of ten smaller than those reported by Waite et al. (2007) due to an error of a factor of 1000 in assumed mass density. These particles at 1,000 km altitude are then precursors to monomers that aggregate to form the larger haze particles observed by optical instruments at 500 km and below. However, considerable microphysical and possibly also chemical restructuring must occur over the altitude range 500–1,000 km if the monomers inferred for the optical haze are composed of aggregates of monomers having radii near 40 nm as determined from the DISR measurements (Tomasko et al. 2009).

12.3.1 Structure Above 400 km from ISS and UVIS

Ultraviolet observations of a stellar occultation provide profiles of aerosol extinction in the altitude range 300–1,000 km. The long-wave (170–190 nm) end of the Cassini Ultraviolet Imaging Spectrograph (UVIS) Far Ultraviolet (FUV) spectrograph was used to measure the extinction of light from the star λ Scorpii as it passed behind Titan's limb. An aerosol vertical profile derived from those data by Liang et al. (2007) is shown in Fig. 12.6. The profile shown in the figure was based on an assumption that the optical extinction can be calculated from Mie theory for spheres with mean radius 12.5 nm and the refractive indices for tholin given by Khare et al. 1984. Both of these assumptions are questionable, especially the assumption that the particles are spheres with radii near 12.5 nm. The important result is that an aerosol signature in the occultation data is present all the way to 1,000 km. The dip in aerosol density just below 500 km altitude is evidence for a thin haze layer in the altitude region 500–520 km.

A thin haze layer often referred to as a 'detached haze' layer was seen in Voyager images and is also seen in Cassini images from 2004 to the time of this writing (2008). Figure 12.7 provides a global view of Titan's haze and shows the change in character of the haze near 55°N latitude (from the Cassini ISS). Rages and Pollack (1983) found a prominent detached haze in Voyager images everywhere south of about 45° latitude and at altitudes 300–350 km and varying with latitude. Porco et al. (2005) report a detached haze just above 500 km altitude and almost independent of latitude below 55° latitude. These differences in altitude are too large to be attributed to measurement error. Rages and Pollack (1983) reported '… a small enhancement in the extinction at −450 km which exists at all latitudes between 75°S and 60°N′. This haze layer may have the same origin as the 510 km layer seen in Cassini images, but it is about 60 km lower. No detached haze is seen in Cassini images between 300 and 350 km and so Titan's haze must have changed in a fundamental way in the intervening years between the observations.

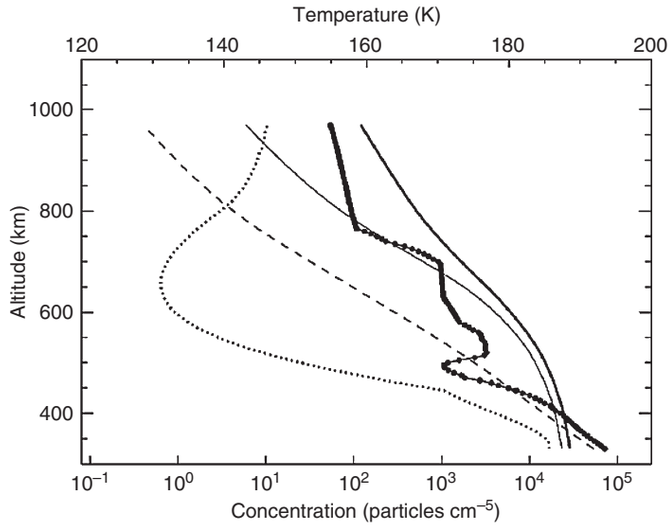

Fig. 12.6 From Liang et al. (2007) Aerosol density (filled circles) derived from the UVIS λ Sco occultation compared to the CH_4 density (dashed line) scaled by 10^{-9} (Shemansky et al. 2005; Shemansky 2006). The increase of the mixing ratio of the UVIS aerosols through the mesosphere to at least 1,000 km implies that the production of aerosols must take place at significant rates throughout the mesosphere and thermosphere. The UVIS-derived temperature profile is shown by the dotted line. Model aerosol profiles computed by Liang et al. (2007) are shown by the thin and thick solid lines

[AU1]

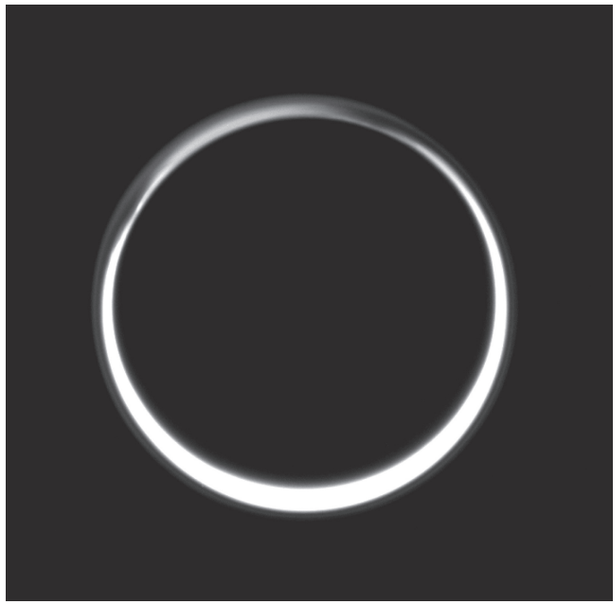

Fig. 12.7 Global view of Titan's stratospheric haze structure. The 'detached' haze layer near 500 Km is seen to be present at all latitudes below 55°N. Titan's spin vector (north) points to about the 11:00 o'clock position

Fig. 12.8 Haze layers at latitudes greater than 55°N show a complex structure which changes over a three-hour period. An MPEG video showing these changes is included in the supplemental DVD

What processes produce a stable (in both time and latitude) thin haze layer in a region of the atmosphere where the sedimentation time is short? Two hypotheses have been discussed. The layer may be a condensation region at a local temperature minimum or it may be a product of non-volatile aerosol formation originating at higher altitude. The condensate hypothesis would provide a natural explanation for the formation of a thin layer provided the location of the haze layer correspond with a local temperature minimum, and that a plausible condensate exists with the abundance and thermodynamic properties to condense at that location. A local temperature minimum is present a little below the haze location in both the in situ HASI (Huygens Atmospheric Structure Instrument) data (Fulchignoni et al. 2005) and the stellar occultation data analyzed by Sicardy et al. (2006). Liang et al. (2007) make the case for condensation of C_6N_2 throughout a broad altitude range in the mesosphere. These particles might serve as condensation nuclei for more complex non-volatile hydrocarbon and nitrile haze material. No condensate candidate has been proposed specifically for the detached layer near 510 km.

The alternate hypothesis, that microphysical processes for non-volatile aerosols originating at higher altitudes (tholins) produce the haze layer, was proposed by Lavvas et al. (2008) who point out that the haze layer coincides with a local temperature maximum just above the temperature minimum in the HASI data and in the stellar occultation (Sicardy et al. 2006) data. They show that local radiative heating by the aerosol layer could produce this feature. They propose that the particles in the detached layer have radii near 40 nm and therefore are the monomers that aggregate and sediment to lower altitude and form the larger aerosols that produce the strong forward scattering of the main haze layer. If this interpretation is correct it provides a significant new constraint on aerosol models – it identities the location where the coagulation of monomers to form aggregates occurs. Some aspects of this detail in the particle microphysics could be tested with existing observations. If the particles in the detached layer are 40-nm monomers their scattering phase functions should not be strongly forward-scattering at visible wavelengths.

Any proposal for the origin of the detached haze should also account for observations of multiple layers and time variations in the vertical structure of the haze in the region between 500 and 600 km altitude. At spatial scales better than about 6 km/pixel some Cassini Imaging Science Subsystem (ISS) images show additional layers above the main 'detached' haze layer, and some show the detached layer to consist of multiple layers. In Figs. 12.7 and 12.8 (West et al. 2008) the 'main' detached haze layer has an intensity peak near 505 km and a secondary peak near 530 km with additional fine structure up to 600 km. It is tempting to attribute multiple layers to the action of inertia-gravity waves (Porco et al. 2005) or by waves forced by tides (Walterscheid and Schubert 2006). These suggestions seem plausible but a detailed model relating wave action to intensity fluctuations remains to be constructed.

Fig. 12.9 From West et al. (2008). Cassini ISS image N1481653824 (UV3 filter). The 'detached' haze layer near 500 km altitude is composed of a main layer near 505 km altitude and additional layers at higher altitudes. This image was taken with the ISS UV3 filter. The image scale is 800 m/pixel. The phase angle is near 160°

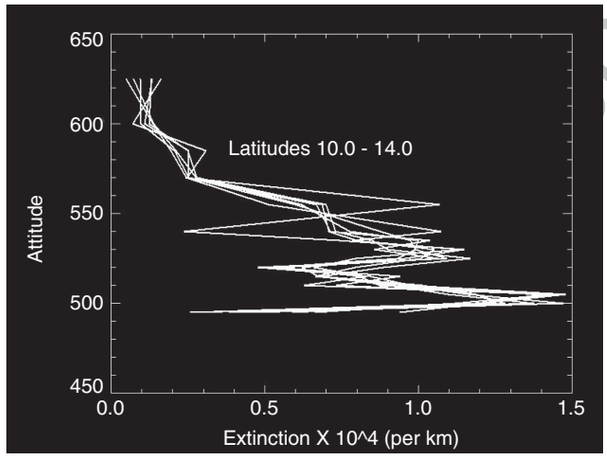

[AU3] **Fig. 12.10** Intensity profiles from Fig. 12.9 were used to retrieve aerosol extinction coefficient profiles for several cuts in the latitude range 10°–14°N Retrievals neglect multiple scattering (from West et al. 2008)

North of about 55°N the haze structure becomes complex and time-variable. Intensity variations occurring on time scales of tens of minutes have been observed in the northern polar vortex region (see the mpeg on the CD). One of the images from that movie sequence is shown in Fig. 12.8. High haze layers are most easily seen at high phase angles and at short wavelengths because of the strong forward scattering and larger scattering cross section at short wavelengths.

12.3.2 Direct Measurements of Titan's Aerosols by Huygens Below 150 km

At altitudes of 150 km and below, the DISR instrument aboard Huygens made direct measurements that constrain the vertical distribution of the haze aerosols. These include measurements by the upward-looking and downward-looking ultraviolet filter photometer (ULV and DLV) which covered the spectral band from 350 to 480 nm, as well as the spectral measurements between 480 and 1,600 nm looking both upward and downward from the Upward- and Downward Looking Visible Spectrometers (ULVS and DLVS) and from the Upward- and Downward Looking Infrared Spectrometers (ULIS and DLIS). All of these measurements were made at many azimuths relative to the direction to the sun. The azimuth of the probe relative to the sun was determined from onboard housekeeping data from a sun sensor as well as from the record of the modulation of the strength of the radio signal received by the Cassini orbiter from the rotating Huygens probe (Karkoschka et al. 2007). Nevertheless, the detailed tip toward the sun and in the orthogonal direction was more difficult to constrain for each observation during the entry. Some of these effects can be seen in the plots of the observations and models in Figs. 12.11 to 12.17.

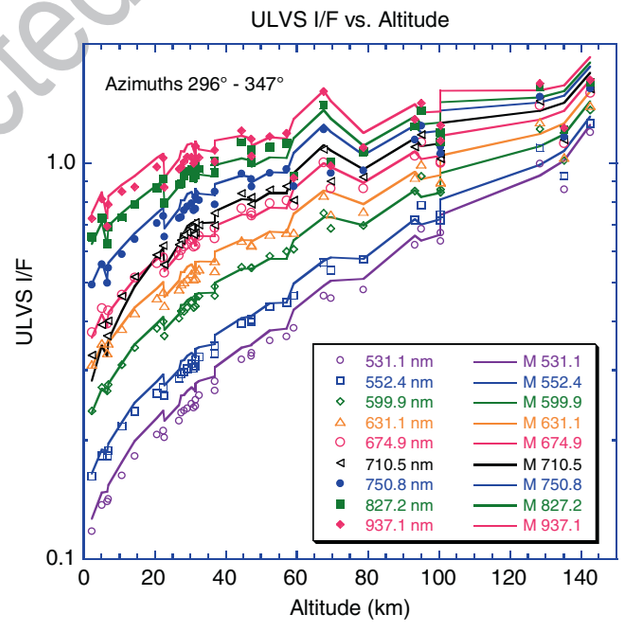

Fig. 12.11 We show the values of I/F measured by the Huygens DISR Upward-Looking Visible Spectrometer as functions of altitude for the instrument pointed at azimuths of 296° to 347° from the sun at nine continuum wavelengths. Measurements at these azimuths included the direct beam from the sun as well as the diffuse radiation from the sky. The measurements (*shown by points*) vary slightly from altitude to altitude due to variations in the exact azimuth of the instrument at different altitudes. The lines are for models computed for the instrument azimuth at each altitude. The variations of the models with altitude and with wavelength are in reasonable agreement with the observations

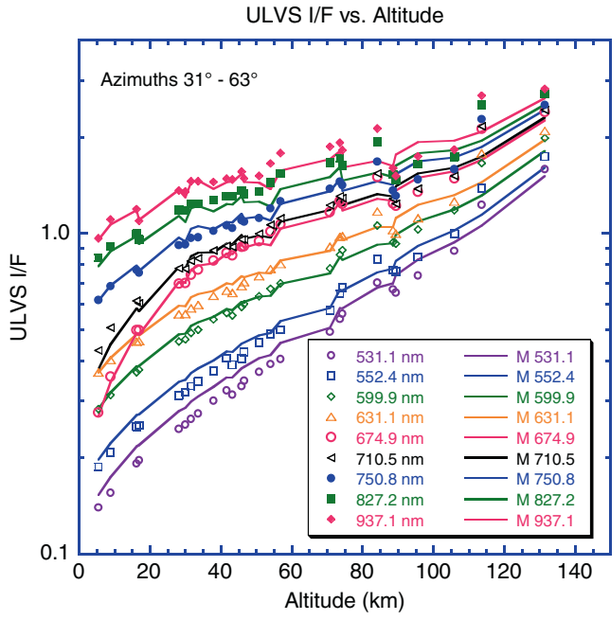

Fig. 12.12 This figure is similar to Fig. 12.11 but is for measurements made when the sun was in a different part of the field of view

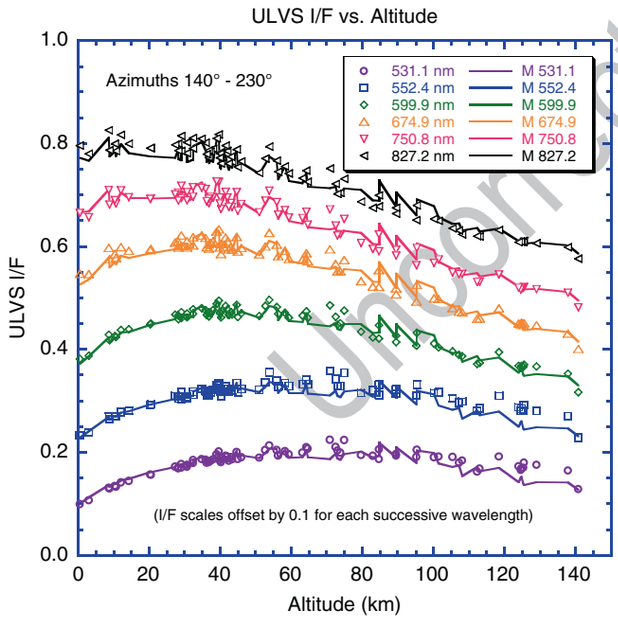

Fig. 12.13 This figure is similar to Figs. 12.11and 12.12 but is for the instrument pointed away from the sun so only diffuse light from the sky is measured. The models fit the diffuse sky brightness reasonably well also

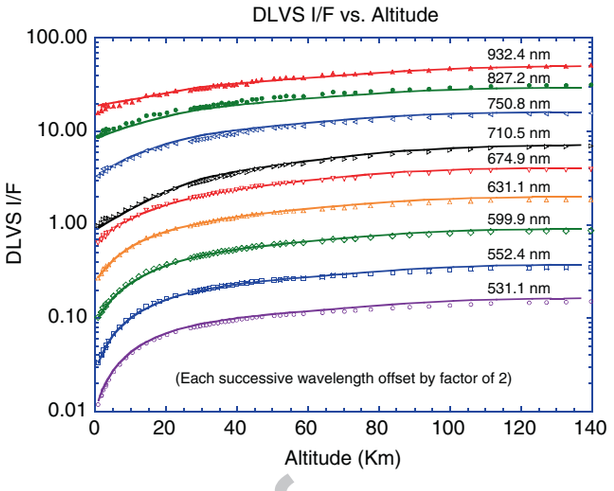

Fig. 12.14 This figure is similar to Fig. 12.13 but is for measurements made by the Huygens DISR Downward Looking Visible Spectrometer averaged over azimuth within a short time at each altitude. The models (*shown by lines*) are in good agreement with the spacecraft observations (*symbols*)

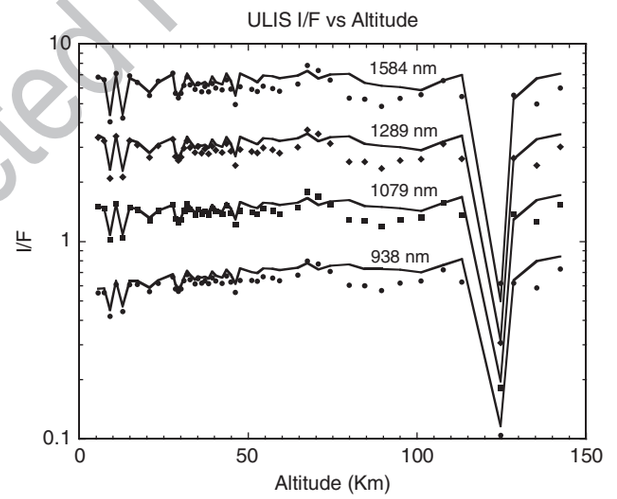

Fig. 12.15 This figure shows the measurements made by the Huygens DISR Upward-Looking Infrared Spectrometer for each 2-min cycle of the instrument during the descent. The measurements are at four continuum wavelengths as labeled. The models shown by lines are for the same set of azimuths at which the measurements were made. The low values near 120 km altitude were when the instrument slowed its rotation rate and reversed direction of rotation. The measurements here were made looking only away from the sun

Despite these complications, the observations of the upward-looking instruments revealed interesting details of the vertical distribution of the haze aerosols. First, no altitude regions relatively clear of aerosols were seen in any altitude intervals. Second, above 80 km altitude, the vertical optical depth of the aerosols had a scale height of about 65 km. Third, between 80 and 30 km, the cumulative extinction optical depth varied linearly with altitude. Fourth, in the lowest 30 km the

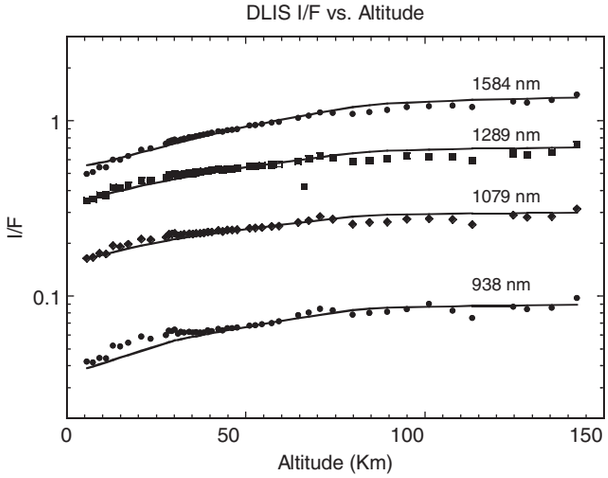

Fig. 12.16 This figure is the same as Fig. 12.15 but is for the Downward-Looking Infrared Spectrometer at the four continuum wavelengths as labeled

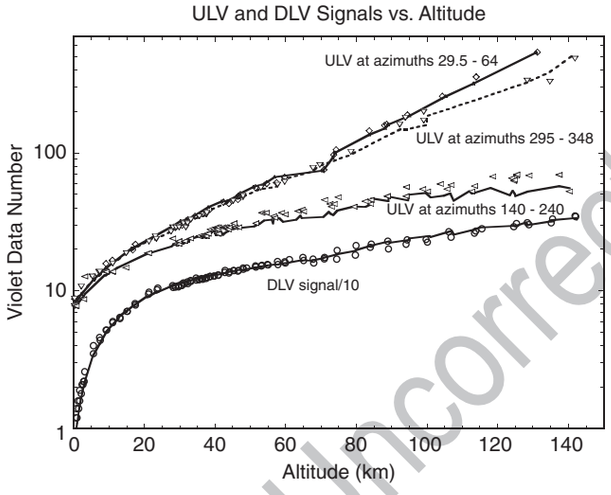

Fig. 12.17 This figure shows the data number measured by the Upward-Looking Violet (ULV) photometer at two azimuths relative to the sun (*diamonds and downward pointing triangles*) compared to models (*solid or dashed lines at the two azimuths*). The measurements of the ULV looking upward without the direct beam are shown by left-pointing triangles. The circles show the measurements of the Downward-Looking Violet (DLV) photometer averaged around all azimuths and divided by 10 to avoid overlap on the plot. The models show good agreement with the observations. The agreement with the altitude variation indicates that the vertical distribution of haze is consistent with the observations, and the agreement of the models with both the ULV and DLV measurements indicates that the variation of single scattering albedo is consistent with the measurements

cumulative extinction optical depth again varied linearly with altitude, although at a slightly different rate than above. The variations of cumulative haze optical depth with altitude at several wavelengths are shown in Fig. 12.18.

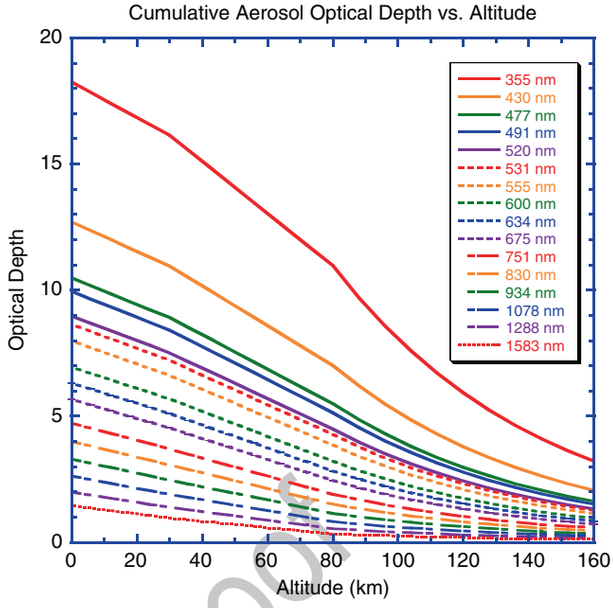

Fig. 12.18 This figure shows the variation of the extinction optical depth of the haze with altitude at several wavelengths, as labeled. No clear regions are seen in the altitude range of the DISR measurements

12.4 Variations of the Optical Properties of Titan's Aerosols with Wavelength

12.4.1 Single Scattering Albedo

The single scattering albedo of the haze aerosols can be constrained by fitting both the upward- and downward-looking observations from the measurements during the Huygens descent. The downward minus upward looking measurements are a measure of the net flux at the altitude of the measurements. The difference in the net flux between two altitudes is due to the solar energy absorbed by the intervening layer and provides strong constraints on the single-scattering albedo. The variations in the energy absorbed with wavelength determine the variations in single scattering albedo with wavelength.

The measurements from the set of optical measurements on DISR are shown in Fig. 12.19 from Tomasko et al. 2008a. These curves result from the measurements over the complete spectral range covered by the instrument. The spectral coverage of each portion of the DISR measurements is indicated by the horizontal lines along the bottom of the figure. Note that two curves are given for the single scattering albedo as a function of wavelength. The significant difference between these curves is an indication that the single scattering albedo of the haze aerosols varies with altitude. Note that the curve for the darker aerosols refers to the higher altitudes.

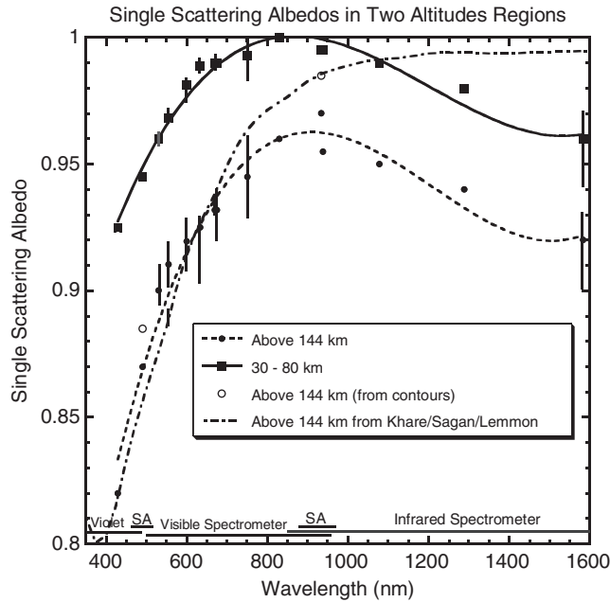

Fig. 12.19 This figure shows the variations of single scattering albedo with wavelength at altitudes above 144 km and between 30 and 80 km, as labeled from Tomasko et al. (2008a). The measurements come from different portions of the DISR data set as indicated by the horizontal lines along the bottom of the figure (Note that SA represents the two channels of the DISR solar aureole camera). The error bars approximate one sigma uncertainties in the derived values. The dotted-and-dashed line is the single scattering albedo computed for the haze aggregate particles using 1.5 times the imaginary refractive index reported by Khare et al. (1984) and shown in Fig. 12.30. The slope toward the blue is in reasonable agreement with the variation of single scattering albedo at high altitudes but does not show the decrease required for the haze aerosols longward of 900 nm

Good fits were found for aerosols with a sharp break in the haze albedo at 80 km, as well as for a gradient in albedo with altitude above 80 km. The curve shown is for a model with fixed albedo above 144 km altitude and a linear gradient in albedo from 144 km down to 80 km. Below 80 km the data require that particles be less absorbing than those at higher altitudes.

The shapes of the curves have two interesting properties. First, the minimum absorption is near 900 nm. Toward shorter wavelengths the absorption increases rapidly. The dotted and dashed curve is for loose aggregate haze particles as determined by the solar aureole camera computed with 1.5 times the imaginary refractive index found by Khare et al. (1984). Note that the slope of the albedo to shorter wavelengths at the highest altitudes is similar. This implies that the variation of imaginary refractive index with wavelength of the haze aerosols must be similar to that measured for tholins.

Secondly, note that the albedo decreases to longer wavelengths after the peak near 900 nm. This occurs both for the aerosols above and below 80 km. This effect also occurs in the reflection spectrum of the surface measured with the DISR surface lamp (Tomasko Tomasko et al. 2005). This may indicate that this feature in the surface spectrum is not due to surface hydrocarbon ices but is due to the coverage of the surface by aerosol material that has settled out of the atmosphere.

Finally, we note that for constraining the shape of the single scattering albedo curve shortward of 600 nm, the measurements used were acquired via a combination of the visible spectrometer, the blue channel of the solar aureole camera, and the ultraviolet filter photometer. Each of these measurements was a difficult challenge for the DISR instrument and resulted in significant error bars to this part of the curve. In fact, when Cassini Visual and Infrared Mapping Spectrometer (VIMS) spectra near the Huygens probe's landing site (Brown et al. 2002) are compared with DISR [AU4] haze models, some adjustment in the shape of the single scattering albedo curve is necessary to optimize the fit. This relatively small difference could be due to calibration differences in the blue portion of the VIMS and DISR instruments, but could also be due to the difficulties in retrieving this portion of the curve in the region where several of the DISR systems overlap.

12.4.2 Single Scattering Phase Functions

Uncertainties in the size of the forward peak in the single scattering phase function results in the inability to determine the true aerosol optical depth because different optical depths are retrieved for different amounts of forward scattering. The shape of the phase function requires measurements at a variety of phase angles, something that is only possible from space missions that can observe Titan over a large range of scattering angles. Observations of the shape of the backward portion of the phase function have been available from the first space missions to the Saturn system during the Pioneer 11 mission (Tomasko and Smith 1982). Pioneer observed the integrated disk over phase angles up to 90° and showed that a modest backward peak was needed for the phase functions in red and blue light. Voyager observed Titan at phase angles up to 150° and showed the need for strong forward scattering from the Titan aerosols (Rages et al. 1983).

The Huygens DISR observations that were acquired at different wavelengths and a range of phase angles during descent through Titan's atmosphere provided constraints on the phase function in several respects. First, observations within 10° of the sun constrained the forward peak at the two wavelengths of the solar aureole camera (491 and 938 nm). The visible spectrometer measured the brightness integrated over a wide field of view looking at various angles from the

azimuth of the sun in both upward and downward directions. The ULVS observations near the sun and opposite to the sun constrain the side-scattering components relative to forward scattering. The downward-looking observations at a variety of azimuths relative to the sun constrain the size of the backward peak in the phase function.

The phase functions used in the DISR analysis were based on fits to phase functions computed for loose fractal aggregate particles and included the polarizing properties of the particles in addition to the intensity. Tomasko et al. (2008a) concluded that loose aggregates were necessary to permit the small size of the aggregates constituent "monomers" to produce the high degree of polarization observed. The authors concluded that the monomer size was approximately 0.05 μm in radius. A more detailed analysis of the DISR polarization analysis indicates that improved fits are actually obtained with slightly small monomers with radii of 0.04 μm (Tomasko et al. 2009).

In order to fit the strong forward scattering pattern, a large projected area of the particles is required. Assuming that the equal projected area radius of a spherical particle representing an aerosol is 2.0 μm, if each monomer has a radius of 0.05 μm, then this requires that 3,000 monomers make up an aggregate particle. A smaller radius of 0.04 μm for the monomers would imply a slightly larger number for the same projected area.

The DLVS observations as functions of azimuth angle relative to the sun show the need for modest backward peaks at wavelengths near 700 nm. At shorter wavelengths, the size of the backward peak decreases. The algorithm used to evaluate the shape of the single scattering phase function from loose fractal aggregates did not produce significant backward peaks in the wavelength range as required. The haze particles near the beginning of the probe measurements (near 150 km altitude) required the lowest single scattering albedos and the ratios of their optical depths with different wavelengths were in the best agreement with the cross section computations for our fractal algorithms. Thus, Tomasko et al. (2008a) limited the addition of the backward scattering peak to altitudes below 80 km, and used the phase functions without the backward peak from the algorithm at higher altitudes. The phase functions at lower altitudes included a smooth backward peak added to the algorithm predictions.

As the wavelength decreased from 700 nm toward blue wavelengths, the size of the backward peak in the phase functions below 80 km was decreased as required by the DLVS measurements as functions of azimuth relative to the sun. Some examples of the wavelength and altitude dependence of the phase functions required by the DISR observations is shown in Figs. 12.20 and 12.21 and can be found in the publication of the DISR analysis (Tomasko et al. 2008a).

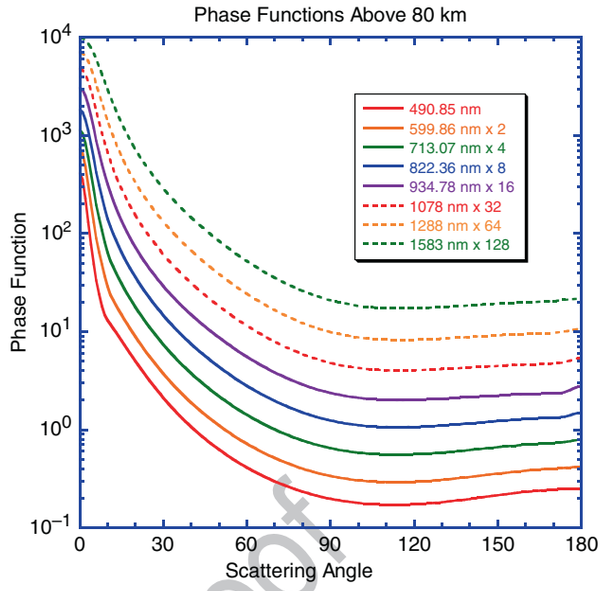

Fig. 12.20 Here we show the shapes of the single scattering phase functions for a range of wavelengths, as labeled. The curves are offset by the factors given in the legend. These phase functions are for the fractal aggregate computations used at altitudes above 80 km

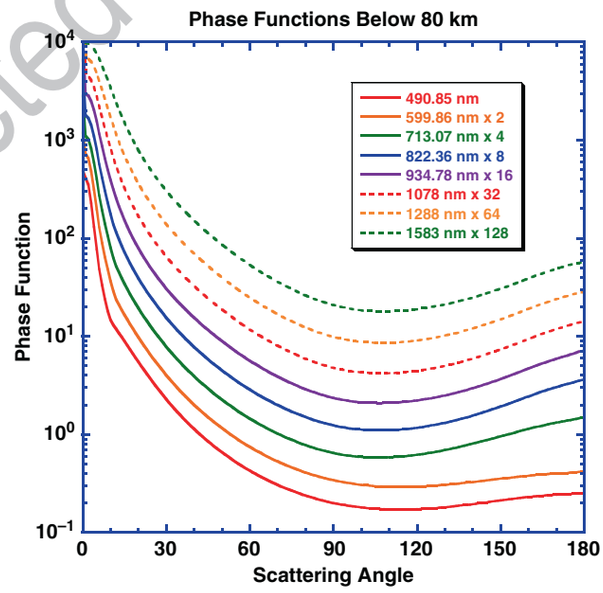

Fig. 12.21 This figure is the same as Fig. 12.20 except it is for the aerosols found at altitudes below 80 km. These curves contain enhances backscattering peaks longward of 600 nm as required by the variation in the DISR Downward-Looking Visible Spectrometer as the Huygens probe rotates

12.4.3 Extinction Optical Depth

The variation of extinction optical depth with wavelength has been shown in Fig. 12.4 and briefly described above.

We noted that the extinction optical depth can be fitted reasonably well with power laws in wavelength, with the steepest slopes at highest altitudes and shallower slopes at lower altitudes, as would be expected for an increase in particle size with depth into the atmosphere. Above 80 km, the extinction optical depth variation with wavelength is in good agreement with the estimates for the fractal algorithm used to describe the haze aerosols, and the aerosol number density as a function of altitude can be reliably determined (see Fig. 12.22). At deeper levels in Titan's atmosphere, the agreement with the predictions for the purely fractal particles worsens, indicating a departure from the purely fractal aggregate particles thought to be present above 80 km. We know that the aerosols at these deeper levels have higher single scattering albedos. This may be caused by condensation of some hydrocarbon gasses onto the fractal particles which may fill some of the voids in the particles, and affect their total cross sections as a function of wavelength.

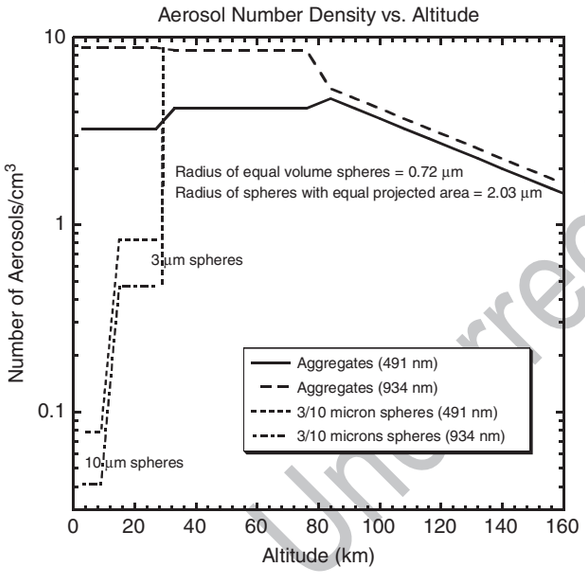

Fig. 12.22 This figure shows estimates of the aerosol number density computed from the cross sections of the fractal haze aggregates and the extinction optical depth profiles at 934 nm (*red*) and 491 nm (*blue*) wavelengths, as labeled. Above 80 km the optical depths and cross sections at the two wavelengths lead to consistent values for number density peaking near 5 particles/cc at 80 km. From 80 to 30 km the number densities derived from the red and blue wavelengths vary by a factor near two, and below 30 km the disagreement is even greater, indicating that the particles differ somewhat from the pure fractal aggregates for which the cross sections are evaluated. Perhaps this is an indication of condensation filling in some of the spaces in the particles. Below 30 km, the optical depth varies only slowly with wavelength, and the cross sections are more nearly constant in red and blue. In this case there is a relationship between the size of larger particles and the number density as indicated by the estimates for spherical particles of 3 or 10 μm radius. For larger particles the number densities in the lowest 30 km of the atmosphere could be one or even two orders of magnitude less that the value of 5/cc found near 80 km

Below 30 km, methane can condense on the particles, which might cause voids in fractal particles to collapse and the density of the aggregate to increase (i.e. to produce shallower variations of cross section with wavelength). However, this cannot happen completely, as the polarization observations in red light at deep levels requires strong linear polarization in single scattering from the haze aerosols even at these low altitudes. It may be possible that some growth in size and some collapse to denser shapes could happen below 30 km that would still permit the observation of polarization as well as optical depth with wavelength to be matched. Unfortunately, no solar aureole observations in red light close to the sun are available from DISR at altitudes below 30 km to test these ideas further.

12.5 Variations in Haze Properties over Titan's Disk

The direct measurements by the DISR instrument on Huygens successfully determined the single scattering phase function, the single scattering albedo, and the vertical variation of cumulative optical depth as functions of wavelength between 350 and 1,600 nm at altitudes below 150 km. It is natural to ask how these properties vary over the disk of Titan, and especially with latitude.

The overall design of the Cassini–Huygens mission plan for Titan was to have the Huygens probe determine the "ground truth" at the landing site and use the remote observations of Cassini to determine the global conditions with the guidance of the Huygens observations at the landing site. Cassini VIMS spectral observations of the landing site as well as over a wide range of latitudes have been analyzed in the past few years and are under current investigation. In this regard, the Huygens observations have been helpful in measuring the absorption by methane at the long paths and low temperatures on Titan for use in the analysis of VIMS observations (Tomasko et al. 2008b). Secondly, remote observations can yield a family of solutions, in that the intensity emerging from the top of the atmosphere can be affected by the vertical variations in phase function, ground albedo, single scattering albedo, and aerosol distribution, and it is often not easy to separate these dependencies. Our goal in this section is to use as much as we can about the haze properties at the landing site and change them only as required to match the VIMS observations at other locations.

First, it should be noted that the haze model determined at the probe landing site from the Huygens measurements with no modifications predicts a spectrum seen from outside the atmosphere that is in good agreement with the VIMS observations of the landing site. This can be seen in Fig. 12.23 where the DISR haze model is used to predict what VIMS

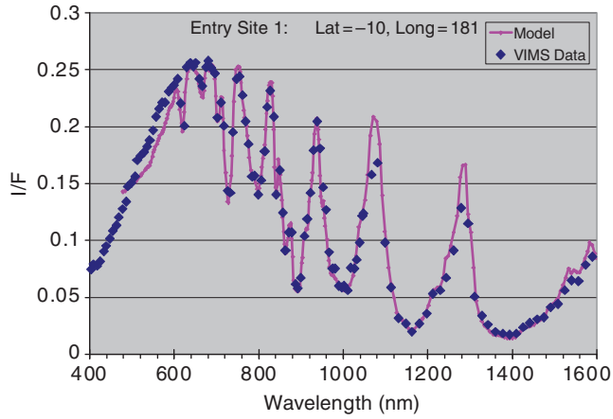

Fig. 12.23 This figure shows Cassini VIMS visible and infrared band measurements (*symbols*) near the Huygens probe landing site compared to a spectrum computed from the DISR haze model (*lines*) at the same scattering geometry. The agreement is good except for the portion shortward of 600 nm

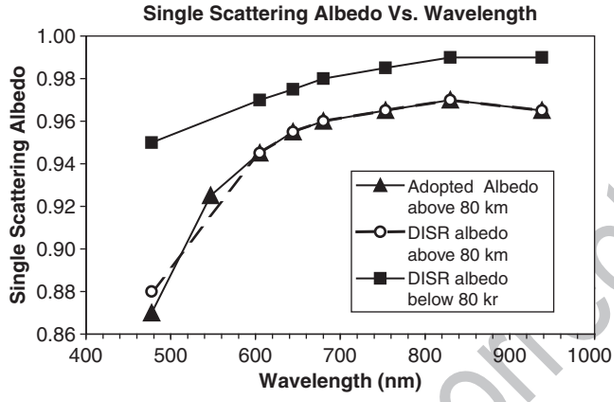

Fig. 12.24 This figure shows the variations of the single scattering albedo used in the DISR haze models above and below 80 km (*circles and squares, respectively*). Below 80 km, no adjustments to the single-scattering albedo curve are necessary to reasonably match DISR model and VIMS data. Above 80 km, a small adjustment in the slopes of the red curves (*triangles and line*) significantly improves the model fit to the VIMS spectra shortward of 600 nm

would see at the landing site. The only change to the DISR haze model needed is a small change in the shape of the haze single scattering albedo shortward of 600 nm (see Fig. 12.24) in a spectral region where DISR has the greatest difficulty measuring this quantity. The improved agreement between the haze model and the VIMS observations are shown in Fig. 12.25. We note further that adjusting only the ground albedo with no adjustment in haze properties or distribution can fit VIMS observations at other longitudes at the latitude of the probe landing.

In addition to the ground albedo, we have found only two further modifications to be necessary to fit VIMS observations over a wide range of latitudes. One is the single scattering albedo of the haze required to match the observed brightness

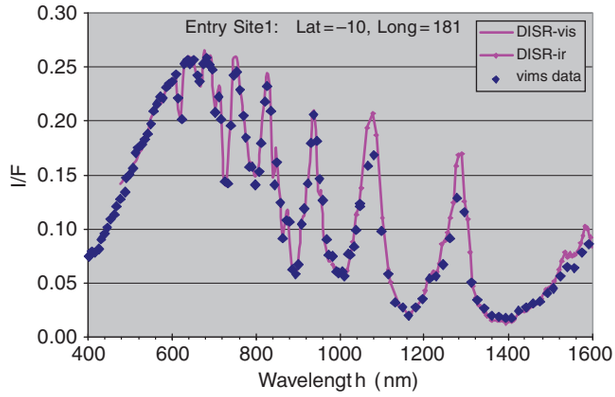

Fig. 12.25 This figure is like Fig. 12.23 except it uses the variation of single scattering albedo above 80 km as given by the triangular points and curves. The fit is quite good throughout

near 600 nm. The haze here is sufficiently thick that the brightness observed is not much affected by the reflectivity of the ground. In the continuum between methane bands, the only way to match the brightness is to change the absorbing properties of the haze. Letting ω be the single scattering albedo of the haze in the DISR model, when the quantity $(1 - \omega)$ is multiplied by the same factor independent of wavelength the model can be adjusted to agree with the observations. Here the absorption in the haze is only adjusted at altitudes above 80 km where the DISR models show the greatest absorption. Below 80 km the absorption in the DISR model is much smaller, and adjustments here make little difference in the brightness seen outside the atmosphere.

The second adjustment is necessary to fit the deep parts of the methane absorption longward of 1,000 nm. These deep bands probe the atmosphere above 80 km. The second factor chosen multiplies the haze optical depth above 80 km. Decreasing the haze here makes the bands deeper, and increasing the factor makes the bands shallower.

It turns out that adjusting only these three parameters (the ground albedo to fit the continuum points longward of 1,000 nm, multiplying the haze absorption above 80 km by a factor, and changing the haze thickness above 80 km) is sufficient to fit VIMS spectral observations shortward of 2 μm wavelength from −60° to +50° latitude. The results are shown in Fig. 12.26 from Penteado et al. (2009). Note that the thickness of the haze shows a steep change at about −10° latitude. North of that latitude, the haze thickness is similar to that at the Huygens landing site. South of that location, the haze above 80 km is only about 60% as thick. The absorption in the haze above 80 km increases slowly with latitude by about 20% in total over the range of latitudes shown. The models require no significant changes to the haze properties or distributions below 80 km. No change in the methane mixing profile from that measured on the probe entry is required to fit the methane bands.

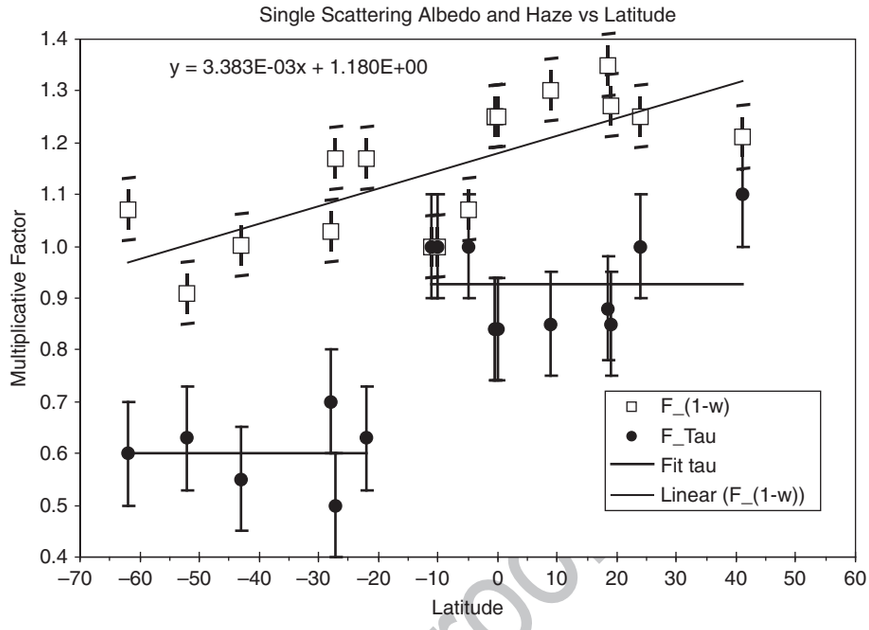

Fig. 12.26 This figure shows the factor (in red) by which (1 − ω) (i.e., 1 minus the single scattering albedo in the DISR haze model above 80 km) must be multiplied to give good fits to VIMS spectra at latitudes varying from 60°S to 40°N. The dark blue points show the factor by which the haze optical depth above 80 km in the DISR haze model must be multiplied to give good agreement to the VIMS spectra at the latitudes shown. North of 10°S latitude, haze parameters in the model are in good agreement with the values measured by DISR. Note that the south of 10°S latitude, the haze is about 60% as thick

The thinner absorbing haze above 80 km combined with the smaller absorption in the haze makes the southern hemisphere appear brighter than the northern hemisphere where the absorbing haze above 80 km altitude is thicker and also more absorbing. These effects are stronger at blue wavelengths and decrease toward the red where the single scattering albedo of the haze above 80 km increases. The effects are similar to those reported in the past for the disk of Titan.

12.6 Seasonal and Long-Term Variations

Lockwood and Thompson (1979) reported on disk-integrated variations of Titan's geometric albedo that they attributed to variations in solar ultraviolet irradiance and its influence on photochemistry. An important clue to the brightness variations was provided by spatially-resolved images from the Pioneer 11 and Voyager 1 spacecraft which showed hemispheric contrast. Sromovsky et al. (1981) noted that the northern hemisphere was darker than the southern hemisphere in violet, blue and green images at the time of the Voyager observations (a little past northern spring equinox). They found four distinct latitude regions, a northern polar zone (north of latitude 55°), a northern mid-latitude zone between 10° and 55°, a southern zone between −20° and −60° and a transition region between −20° and +10°. This configuration is quite similar to what the Cassini instruments found between 2004 and 2008 (between southern summer solstice and northern spring equinox). Sromovsky et al. (1981) proposed that seasonal variations in Titan's global circulation pattern and its effect on the distribution of haze produce the hemispheric differences and dominate the variations reported by Lockwood and Thompson. The substantial phase lag of the reflectivity asymmetry relative to hemispheric asymmetry in the solar heating rate supports this idea because of the long radiative time constants of the lower atmosphere which contains most of the atmospheric mass (see Chapter 12).

Some clues to the relationship between aerosol microphysics and reflectivity asymmetry are provided by observations using the Hubble Space Telescope and the Cassini orbiter instruments. Lorenz et al. (1997) studied spatially-resolved images from the Hubble Space telescope in the period 1990–1995 (leading up to southern spring equinox). They showed that contrast in the strong methane band near 890 nm is in the opposite sense as contrast in the blue. Hemispheric asymmetry during the period 1992–1995 was the reverse of the asymmetry pattern observed during the Pioneer and Voyager epochs. Curve fitting performed by Lorenz et al. (1997) predicts that north/south hemispheric ratio observed by Cassini instruments should reach an extremum (about 0.8 at blue wavelengths) near northern spring equinox in 2009 and reverse near northern summer solstice in 2017. Lorenz et al. (1977) proposed that hemispheric [AU5] contrasts are due to aerosol microphysical variations in the region above 70 km altitude and mostly below 120 km altitude driven by seasonal variations in aerosol transport by wind, in agreement with (but more specific than) the view that Sromovsky et al. (1981) put forth. Karkoschka and Lorenz (1997) derived haze aerosol radii near 0.3 μm in the northern latitudes versus 0.1 μm in the south in from 1995 HST images of Titan's shadow on Saturn. They assign these particle radii to different layers, the 'detached haze' layer at northern latitudes and the main haze layer at latitudes south

of −50°. The high southern latitudes would correspond to a southern polar vortex regime.

The axis of symmetry generated by the hemispheric contrast in the haze is not aligned with Titan's spin axis. Roman et al. (2009) found a small tilt (4.1° +/− 0.3°) between the two from Cassini ISS images. The tilt is consistent with a similar offset in the axis describing symmetry of the temperature field as sensed by the Cassini CIRS data (Achterberg et al. 2008). These observations were unexpected from general circulation models of Titan and may provide an important clue to the mechanism responsible for Titan's super-rotation.

12.7 Role of Aerosols in Titan's Heat Balance

Knowledge of the haze structure and optical properties at wavelengths from the near ultraviolet to the near infrared permits computation of the net flux of sunlight as functions of altitude and solar zenith angle. These permit computation of the solar heating rate as a function of altitude averaged around circles of latitude to average over a Titan day. Further, Cassini's Composite Infrared Spectrometer (CIRS) observations at thermal infrared wavelengths can be used to obtain the thermal cooling rate as functions of altitude. These can be averaged and combined with the solar heating rates to give the net radiative heating or cooling rate as a function of altitude averaged around circles of latitude. As of the date of this book, this has only been done for the 10°S latitude of the Huygens probe entry. Figure 12.27 from Tomasko et al. (2008c) shows the results of the heating and cooling rate

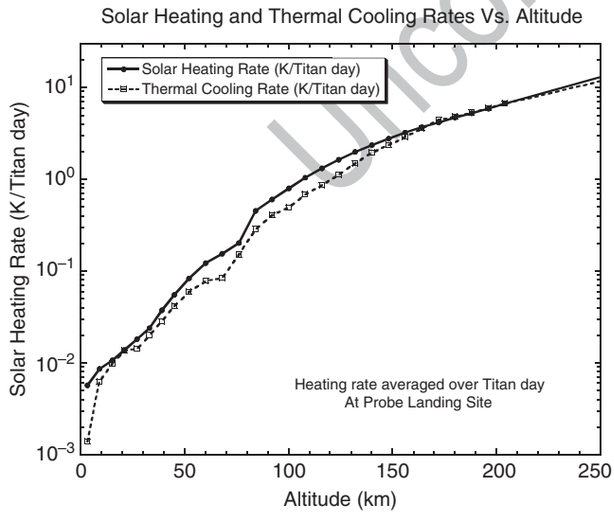

Fig. 12.27 This figure shows the solar heating rate and thermal infrared cooling rates as functions of altitude averaged around Titan in a small band 10°S latitude near the Huygens probe landing site. The heating and cooling rates were computed using aerosol, gas composition, and temperature profiles from DISR and CIRS observations by Tomasko et al. (2008c)

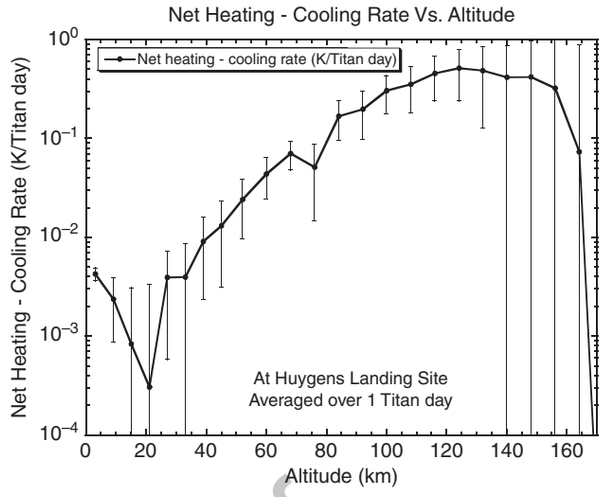

Fig. 12.28 This figure shows the net radiative heating rate (*solar heating minus infrared cooling*) as function of altitude averaged around all longitudes on Titan near 10°S latitude. Note that the net heating rate peaks near 0.5 K/Titan day near 120 km altitude and decreases toward higher and lower altitudes

calculations for this location. Note that the solar heating rate slightly exceeds the thermal cooling rate. The excess is shown in Fig. 12.28. Because there is no evidence that the thermal structure of this region is changing, dynamical motions must redistribute this heat to other regions on Titan. These computations need to be repeated for other latitude circles to define the net radiative forcing for dynamics. We can anticipate that this will be done in the near future using the continuing observations from the Cassini orbiter.

12.8 Haze Microphysical Models

Authors attempting to determine the optical properties of Titan's haze must cope with the large number of parameters needed to describe the haze including the single-scattering phase function, albedo, cross sections, size, shape, and the variations of these properties with wavelength as well as with altitude. It is useful to apply physical constraints to decrease the degrees of freedom to a smaller number that might actually be constrained by existing observations. Among the first of these studies was that by Toon et al. (1992). These authors assumed that Titan's aerosol particles had a spherical shape, and used a one-dimensional model to combine a parameterized mass production rate, sedimentation, coagulation, and eddy diffusion to constrain aerosols properties. While limited to considering spherical particles, this study led to several interesting conclusions. The authors noted that the large variation in optical depth of the haze implied that small particles would fall out of the atmosphere slowly. They noted that

eddy diffusion must increase vertical motions considerably above that produced by sedimentation to limit the vertical optical depth to reasonable values. They also noted that vertical motions of the order of 1 cm/s could cause features such as the detached haze layer and that small motions of the order of 0.05cm/s could produce significant hemispherical asymmetry. The authors pointed out that coupled two-dimensional models were likely to be required for more precise conclusions.

Shortly after this work West (1991) suggested fractal aggregates for the shape of the aerosols, and West and Smith (1991) showed that such particles could reconcile the measurements of high polarization and strong forward scattering.

In 1992, Cabane et al. (1992) published the first microphysical models that incorporated fractal aggregates. They showed that the aerosols could be divided into two regions, a region where the monomers were formed and continued to grow by the largest particles sweeping up the smaller particles followed below by a region where the monomers combined to form fractal aggregates. They found that the monomer size was relatively independent of electrical charge, mass production rate, and eddy diffusion and depended primarily on the altitude of formation since the density of gas at this altitude determined the time particles of various sizes could be suspended and grow. They also concluded that treating the monomers as spheres was a good approximation since the monomers grew by incorporating many smaller particles from the gas.

This work was followed by a paper by Cabane et al. (1993). In this paper the authors addressed the problem of how the aggregates were assembled, and how the number of monomers in the aggregates varied with altitude for different altitudes of the production region. They noted that the settling speed of the loose cluster-cluster aggregates is independent of the mass of the aggregate and is the same as the settling speed of the individual monomers. Using the suggestion of West and Smith (1991) that the aggregates each contain 8 monomers of radius 0.06 μm, the models were adjusted to give reasonable agreement with these values. They found that the production zone must be 350–400 km to give the required monomer size and an effective radius of the aggregates of 0.3 to 0.5 μm to satisfy the forward scattering constraint from the high phase angle observations of Voyager.

Assuming the charge on the particles was 30 electrons/μm, they found the monomer size to be affected little by the charge and that the monomer size depended mostly on the altitude of formation.

They noted that for production altitudes near 500 km, the number of monomers per aggregate would be larger than 500, values that seemed inconsistent with the results of West and Smith (1991). Both Toon et al. (1992) and Cabane et al. (1993) ascribed the presence of aerosols at higher altitudes (as in the detached haze) to dynamical motions.

These studies of the microphysics of fractal aggregates were followed by attempts to fit the geometric albedo of Titan with these types of particles by Rannou et al. (1995). These authors use a microphysical model for the properties and vertical distribution of the aerosols, an approximate treatment to evaluate the cross sections and asymmetry parameter of the haze particles, and a two-stream radiative transfer code to attempt to fit the geometric albedo of Titan from 0.2 to 1 μm wavelength.

In order to permit relatively accurate computations of the optical properties of the aerosols, the authors concentrated on using a production altitude of 535 km, higher than the 350 to 400 km determined from previous studies, to give monomer sizes of 0.03 μm that were sufficiently small to permit relatively good agreement with the geometric albedo down to 0.2 μm wavelength.

They varied the aerosol production rate, the electric charge of the aerosols, the imaginary refractive index, the methane abundance, and the fractal dimension of the aggregates. When the fractal computations were compared to models using spheres, they found that even compact fractal particles behaved significantly differently from spheres in that the particles reached greater optical depths at higher altitudes and had less forward scattering phase functions than the Mie particles. Both effects helped to provide the very low geometric albedo of Titan needed at short wavelengths.

They also found families of solutions where increases in the aerosol mass production rate could be compensated by changes in the methane abundance in the visible and near infrared (IR) part of the spectrum. They found that the fractal dimension of the aerosols was not well constrained by the observations, with values between 1.8 and 3 being capable of yielding fits. Nevertheless, they found that the fractal models were able to fit the low UV albedo without the ad hoc addition of very small particles used by some previous authors.

Hutzell et al. (1996) were the first to use a two-dimensional haze model together with two different estimates of the circulation on Titan to explore the effects of dynamical haze transport on the variations of Titan's reflectivity from the ultraviolet to the near infrared as functions of season and latitude. In this study, they did not have a fully coupled model in which the changing haze distributions varied the forcing for the dynamics. Nevertheless, they were able to reach several useful conclusions about the interaction of dynamics and haze and reflectivity.

These authors used two different and fixed dynamical circulations to explore the implications for the haze distribution. One dynamical circulation model was a simple Hadley cell, while the other was the result of a general circulation model in which the heating due to absorption by the haze was constant. They concluded that wind fields of the order of 1 cm/s can have significant effects on the albedo and can

produce variations in the geometric albedo of Titan with time that have approximately the same magnitude as are observed by Cassini. They noted that variations due to haze production rate alone did not produce sufficiently large variations.

However, neither of the two circulation patterns they used was able to produce the observed variations of albedo with latitude that are relatively constant in each hemisphere with a relatively sharp transition at low latitude. They concluded that the Titan circulation must be broadly uniform in each hemisphere and have a sharp transition to reproduce the observations. A coupled haze-dynamical model would be needed in which the dynamical forcing changed in response to changes in the haze distribution.

Finally, the authors pointed out that the composition of the haze could also change with latitude and season, and a coupling of the chemistry that produced the haze needed also to be added to the model.

Rannou et al. (2003) used measurements of several different types including the geometric albedo spectrum from the ultraviolet to the near IR, the measurements of high linear polarization and strong forward scattering, and the profile of extinction observed at high altitudes together with a one-dimensional microphysical model for fractal aggregates to constrain the vertical profile of aerosols as well as the monomer size and number of aggregates in the haze particles. They used variations in the aerosol mass production rate, the electrical charge on the particles, the eddy diffusion profile, and the methane mixing ratio to fit the observations.

They found that increasing the eddy diffusion coefficient smoothed the aerosol profile and generally required larger aerosol mass production rates to match the methane bands. For the small values of the eddy diffusion coefficient they used, they reported an aerosol mass production rate near 0.7×10^{-14} g cm^{-2} s^{-1}.

The use of fractal aggregates for the shape of the aerosols easily permitted the observations of high linear polarization and strong forward scattering to be matched. They explored monomer radii between 0.04 and 0.095 μm. They excluded monomer radii greater than 0.075 mm because they did not permit fits of both the low UV albedo and the 619 nm methane band for any combination of mass production rate and eddy diffusion coefficient. It is expected that monomer radii larger than 0.075 mm would have difficulty fitting the high measured polarizations also. The authors pointed out that because the cross sections of the aggregates varied approximately with the number of monomers, the optical properties of the aggregates did not vary much with monomer number. In contrast, the optical properties of the particles depended more sensitively on monomer size.

Rannou et al. (2003) reported that one of the main difficulties was simultaneously fitting the strong methane band at 890 nm and the weaker band at 690 nm. In order to limit the depth of the 890 band to the observed value, a significant amount of haze had to be located above 80 km altitude. In the normal microphysical calculations, the optical depth per unit of altitude (the aerosol extinction) was expected to increase with depth into the atmosphere. However, once the haze optical depth was sufficiently large to fit the 890 nm band, the extinction had to decrease at low altitudes to permit photons to reach deep atmospheric levels where the 690 nm band was formed. The authors noted that several other workers reported a need for the aerosol extinction to decrease at low altitudes also.

These results must be reviewed in light of the new values of the methane absorption coefficients derived for the 890 nm methane band from the Huygens observations. Tomasko et al. (2008b) noted that the absorption coefficient for the 890 nm methane band is overestimated in the Karkoschka (1998) determination that has commonly been used in such work. With the newer lower values of the methane absorption in the 890 nm band from the Huygens observations at large paths and at low temperatures, less aerosol extinction is needed high in the atmosphere to match the observed depth of the 890 nm band than previously thought. In this case, the decrease in extinction at low altitudes to match the weak 619 nm band would be smaller than in the past.

Two relatively recent studies of microphysical processes in Titan's atmosphere have appeared since the entry of the Huygens probe into Titan's atmosphere. In one, Bar-Nun et al. (2008) compared the monomer size and aerosol density predicted from their model to that observed by the DISR instrument on Huygens. They found good agreement between the monomer size predicted by their model (0.04 μm) and the value published by Tomasko et al. (2008a) of 0.05 μm. Remarkably, recent further analysis of the DISR polarimetry in Titan's atmosphere has led to a slight revision of the monomer size to a value even closer to the value predicted by the Bar-Nun model (Tomasko et al. (2009).

A new study by Rodin et al. (2009) also investigated the [AU6]
microphysics of Titan's fractal aggregates and made a detailed comparison with the optical measurements made by DISR looking upward and downward in Titan's atmosphere over the visible and near IR spectral range. These authors found that a Coulomb barrier that limits the Brownian aggregation of small tholin particles possessing a single elementary charge primarily determined the monomer size of about 0.05 μm. In contrast to the earlier microphysical studies, they believed that the monomer size was controlled by the electrical charge rather than primarily by the altitude of formation.

Finally, a recent investigation by Lavvas et al. (2008) used a combination of observations by the Cassini imaging system (ISS), the UV spectrometer (UVIS), and the Huygens atmsopheric structure instrument (HASI) to determine the number density, size, and mass flux near the location of the detached haze layer at 520 km altitude. They find that aerosol

radii of about 40 nm above this altitude are capable of producing the locally higher temperatures just above the location of the detached haze layer seen in the HASI temperature profile. Their aerosol profile is also consistent with the UVIS profiles. Their mass flux of 1.9 to 3.2 × 10^{-14}g $cm^{-2}s^{-1}$ is about the same as required for the main haze at lower altitudes. They suggest that the 40 nm particles are formed at altitudes up to 1,000 km by absorption of solar photons at wavelengths of <145 nm through radical and ion chemistry. They find that the lower apparent aerosol density in the detached region is due to the aggregation of the 40 nm monomers above to particles that fall faster and cause a local decrease in slant aerosol opacity at 520 km altitude. They estimate that the number of monomers in the aggregates at lower altitudes is of the order of 1,000. Their estimates of the size of the monomers and the number of monomers in the aggregates at lower altitudes are in good agreement with the measurements made by the Huygens probe (Tomasko et al. 2008a). Because the mass production above and below the detached region is the same, they believe that the real source of the haze material is due to the radical and ion chemistry at very high altitudes up to 1,000 km and not due to neutral chemistry driven by methane photolysis at lower altitudes of 300 to 500 km as been previously suggested. This work suggests that we may be beginning to understand the type of mechanisms that produce the aerosol material, the location where it is produced, and how it grows to monomers and then aggregates at lower altitudes to exhibit the sizes, shapes, number densities, and vertical distributions observed in the full suite of Cassini/Huygens observations.

12.9 Laboratory Simulations of Titan's Aerosols

Due to the difficulty in producing in the laboratory the physical and chemical conditions and the relevant time scales of the Titan atmosphere it is not obvious that laboratory studies of Titan's haze would yield meaningful results. In spite of the difficulties laboratory work has served to guide our understanding and even emboldened us to think in new ways about the optical, physical, and chemical properties of the aerosol particles.

12.9.1 Early Tholin Production and Optical Properties

Laboratory work on Titan haze dates back at least to 1979 (Podolak et al. 1979) when it was known that haze particles are strongly absorbing at blue wavelengths and that photochemistry initiated by methane photolysis was likely to be the starting point for haze formation. Soon afterward analyses of Pioneer and Voyager data showed that Titan haze particles are both forward scattering and highly polarizing at middle scattering angles. Attempts to reconcile these properties with distributions of spherical particles failed, leading to the suggestion that the particles are nonspherical (West et al. 1983). Laboratory experiments by Bar-Nun et al. (1988) established that polyacetylene and polyhydrogen HCN particles form semi-liquid small spheres or deformed spheres with sticking coefficient near 1, and that these monomers naturally form aggregate particles (Fig. 12.29). However, the size of the monomers in the laboratory simulations was larger than found for Titan and the number of monomers which formed the aggregate was lower. In retrospect these differences may be due to the charge on the aerosol that might limit the growth of the monomer and was not matched in the laboratory.

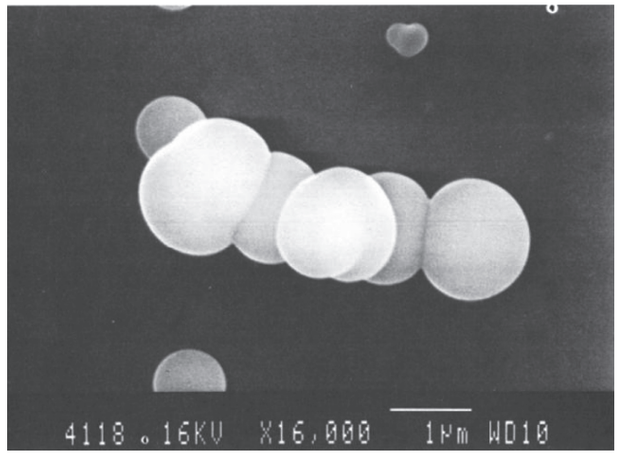

Fig. 12.29 From Bar-Nun et al. (1988). Scanning electron microscope pictures of an aggregate of polyacetylene aerosol particles, demonstrating their semiliquid nature

Laboratory work on tholins in a variety of environments began at Cornell University in the 1970s (Sagan and Khare 1979). Khare et al. (1984) published a seminal paper on the optical constants of Titan haze analog. The values for refractive index they derived are shown in Fig. 12.30. Those values faithfully reproduce the spectral shape of the haze absorption over the visible part of the spectrum out to about 0.8 μm, but between 1 and 1.6 μm the laboratory results are not as absorbing as the DISR data indicate (Tomasko et al. 2008a).

12.9.2 Summary of Some More Recent Laboratory Investigations

Experimental studies of Titan haze analogs continue up to the present. Here we mention a few key results to indicate

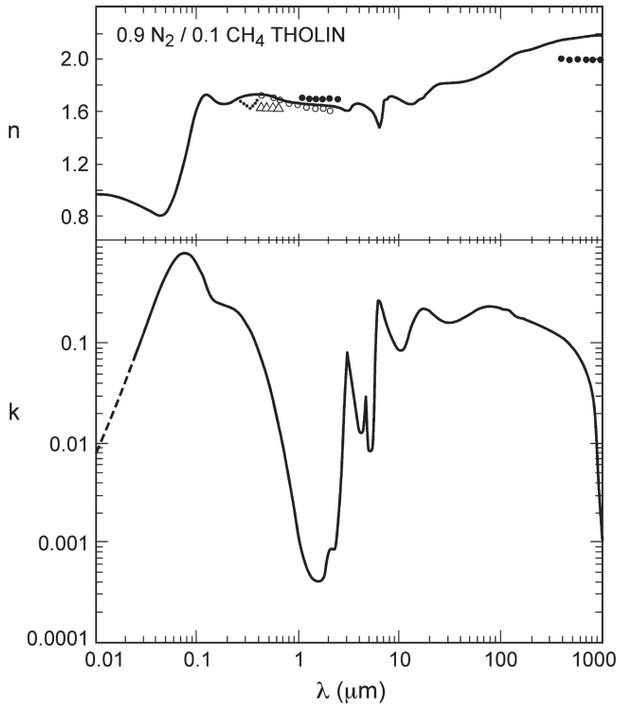

Fig. 12.30 From Khare et al. (1984). The real (n) and imaginary (k) refractive indices for laboratory tholin produced in a plasma discharge for a starting mixture of 0.9 N_2 and 0.1 CH_4

which questions are under investigation and which groups are active in this area.

Optical constants of material derived from laboratory simulations have been reported by Ramirez et al. (2002) and by Imanaka et al. (2004). These papers explore a range of physical and chemical regimes (methane mole fraction, pressure during haze formation). Optical constants are reported in the wavelength range 200–1,000 nm. The variety of tholin materials formed under different conditions all have imaginary index k decreasing from UV to IR wavelengths but the Khare values are almost always higher than the others, sometimes by an order of magnitude. The real part of the refractive index is also highest for the Khare et al. work over most of the wavelength range.

Energy supplied by solar UV photons is likely to dominate the energetics leading to haze formation, although energetic particle bombardment from Saturn's magnetosphere can also make a contribution. The processes are more complex when one considers that photons generate photoelectrons and that ion-neutral chemistry operates on a much faster time scale than does neutral chemistry alone. Additional complexity arises from the fact that photons penetrate to different levels in the atmosphere depending on the wavelength and the dominant processes vary with altitude, with the longest wavelengths penetrating deepest and acting on previously-formed large molecules, whereas shorter wavelengths are absorbed at high altitude and operate on simple molecules as well as more complex ones. The more recent studies investigate the relative importance of the various processes. More focus is also being placed on the fate of aerosols on the surface and their possible interaction with surface water, a condition that can lead to the formation of amino acids and other organic molecules of importance in a pre-biotic or proto-biotic environment.

A substantial laboratory effort has been underway at the Laboratoire Interuniversitaire des Systèmes Atmosphériques (LISA) in Paris. Some of the work was summarized by Coll et al. (2001) who described the experiment and noted that C_4N_2 has been detected. They also reported on particle shape and size, solubility in hydrocarbons and nitriles, chemical composition, and optical behavior in the 200–900 nm wavelength range. Nguyen et al. (2008), also from LISA, showed that aerosols probably do not lead to isotopic fractionation, and they discussed hydrolysis of tholin material on the surface.

Curtis et al. (2008) investigated the role of haze as condensation nuclei for methane or ethane and found that supersaturation of ethane is more likely than that for methane. They also found results for ethane that are consistent with the observation of a polar ethane cloud (Griffith et al. 2006). Release of adsorbed methane and other volatiles from haze particles on the surface may also account for the rise in mixing ratios of those constituents observed by the Huygens Gas Chromatograph and Mass Spectrometere (GCMS) after landing (Nieman et al. 2005). Signorell and Jetzki (2007) [AU7] commented on the crystalline state of methane ice particles. Adsorption aids nucleation.

Other recent results are worthy of mention. Our list is not exhaustive but it shows the range of work being done. Bernard et al. (2006) examined reflection spectra of two types of tholin classified as possible end members of relevance to surface composition. They used near-IR, visible and UV-Raman techniques. Ultraviolet Raman signatures offer the potential to identify aromatics. McGuigan et al. (2006) looked at compounds emitted by pyrolysis of tholin using a two-dimensional gas chromatograph (GC × GC) with a time-of-flight mass spectrograph. They found low-molecular-weight nitriles, alkyl substituted pyrroles, linear and branched hydrocarbons, alkyl-substituted benzenes and PAH compounds. Tran et al. (2008) found that the addition of HCN to the basic gas mixture (which includes N_2 and CH_4) does not significantly affect the optical properties of the haze. Imanaka and Smith (2007) explored the role of [AU8] photochemistry stimulated by photons in the wavelength range 50–150 nm, at higher energies than used by other studies. This work is relevant to high altitudes (near 1,000 km) where Waite et al. (2007) found surprisingly complex chemistry thought to be the starting point of haze formation (see Chapter 7).

12.10 Condensation Clouds

There are two fundamentally different types of cloud systems: (1) tropospheric clouds, dominantly methane ice and probably convective, and (2) stratospheric clouds composed of trace organic ices (hydrocarbons and nitriles), probably cirrus-like and statically stable. The main source for the former appears to be the surface, and clouds are formed during atmospheric up-welling. The source for the latter is photochemistry in the mesosphere and thermosphere coupled with atmospheric down-welling due to diffusion and general circulation. Sagan and Thompson (1984) listed many photochemical products which might condense near the temperature minimum (at altitudes between 50 and 100 km). Ethane is probably a member of both of these groups (Barth and Toon 2006). We begin by discussing the first group.

12.10.1 Methane/Ethane Tropospheric Condensate Clouds

We now have observational evidence from both ground-based and spacecraft experiments for condensates near and below the temperature minimum. An east/west limb brightness asymmetry was discovered in ground-based near-infrared images and spectra (Ádámkovics et al. 2007). The asymmetry is subtle and therefore the amount of material involved is probably small. Ádámkovics et al. (207) infer that methane ice particles at an altitude of 30 km (below the temperature minimum) over the Xanadu region, are responsible for the asymmetry, and that a methane ice drizzle is present at lower altitude. The asymmetry also implies a slight cooling during the night at the altitudes where condensation occurs.

The methane 'hydrologic' cycle is a fascinating topic whose scope is largely beyond the space available here. Evidence for fluvial erosion is abundant from the widespread distribution of dendritic channels (see Chapter 4), but condensate clouds are rarely seen, especially at low latitude. The atmosphere contains a large amount of methane that may precipitate episodically and torrentially but only briefly (See Chapters 12 and 13) Another (antithetical) mode of precipitation has also been proposed: rain without clouds (Toon et al. 1988). We focus here on the observations of condensate clouds.

The first indications that condensate clouds form and dissipate in sufficient mass to be sensed with whole-disk spectrophotometry came from the ground-based observations of Griffith et al. (1998). Later, ground-based adaptive optics images were able to resolve locations of cloud fields (Brown et al. 2002; Roe et al. 2002 and subsequent papers). Observations in the years just prior to the first detailed observations by Cassini showed clouds occur predominantly at high southern latitudes (Schaller et al. 2006). Southern polar clouds appeared during the first Cassini Titan flyby in July 2004. At an image scale near 2 km/pixel the Cassini ISS images revealed south polar cloud detail and morphology similar to that for terrestrial cumulus clouds (Fig. 12.31, frames a–d). Substantial evolution of the cloud field was observed over the 4.5-h observation period. Cassini ISS observations of the cloud field in filters that sample methane bands of different strengths in the near-infrared and visible, and at nearby continuum wavelengths are consistent with methane ice clouds high in the troposphere (see Fig. 12.32). Ground-based observations are also consistent with this interpretation (Brown et al. 2002).

The latitudinal distribution of condensate clouds might provide a strong constraint on atmospheric circulation models and the methane hydrological cycle. Between 2001 and the end of 2004 almost all clouds were in the high southern latitudes. Beginning in December of 2004 ground-based

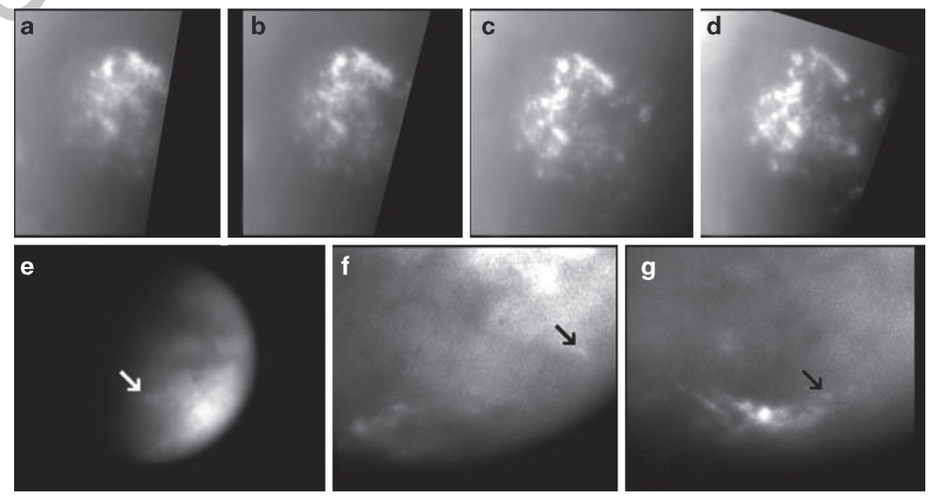

Fig. 12.31 From Porco et al. (2005). Tropospheric cloud features on Titan. Panels a–d: a sequence of four methane continuum images showing the temporal evolution over the period 05:05–09:38 of the Titan south polar cloud field on 2 July 2004. Panels e–g: three examples of discrete mid-latitude clouds (arrows) for which motions have been tracked. Coordinates are as follows. Panel e: 388 S, 818W (29 May 2004); f: 438 S, 678W (23 October 2004); g: 658 S, 1108W (25 October 2004)

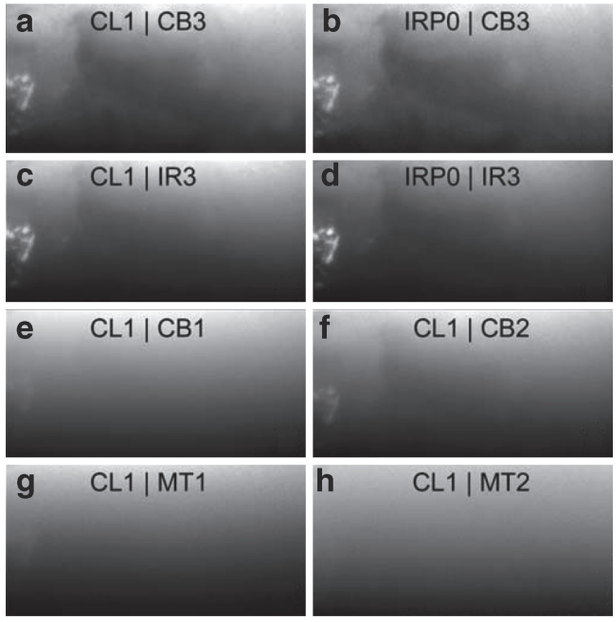

Fig. 12.32 From Porco et al. (2005) Near-simultaneous images of Titan's south polar clouds acquired on 2 July 2004 in eight filter combinations, as indicated by the legend at the top of each image. The high-contrast cloud field on the left of each image is located near the south pole. For each image, a spectral bandpass filter was combined with either a clear filter (CL1) or an infrared polarizing filter (IRP0), which helps reduce obscuration by the overlying stratospheric haze. Filters are as follows: Narrowband methane continuum images (CB3, 938 nm) without (**a**) and with (**b**) the polarizing filter. Broadband infrared (IR3, 928 nm) images, without (**c**) and with (**d**) the polarizing filter. Narrowband continuum images CB1 (635 and 603 nm; **e**) and CB2 (750 nm; **f**). (**g, h**), Methane band images in weak (MT1, 619 nm; **g**) and moderate strength (MT2, 727 nm; **h**) bands. Both clouds and apparent surface features are visible in CB3 and IR3 and to a lesser extent in CB2 and CB1, for which obscuration by stratospheric haze is stronger. In MT1, all features except the polar clouds have disappeared. Gas absorption alone is sufficient to ensure that fewer than 1% of MT1 photons reach the surface, and haze scattering reduces this further. The cloud is barely visible in MT2, which has essentially no contribution from the surface

monitoring found only a few clouds at high southern latitude (Schaller et al. 2006; see Fig. 12.33). Clouds are also observed near latitude −40° (Turtle et al. 2009). To explain the preponderance of cloud occurrences at high southern latitude Brown et al. (2002) proposed that solar heating of the surface layers is important in initiating the chain of convective activity that results in cloud formation. Observations of surface temperature from Cassini instruments do not support this view. Brightness temperatures at south polar latitudes are cooler than elsewhere (Jennings et al. 2009). Large-scale circulation is probably the more important driver. Upwelling or a strong latitudinal temperature gradient might provide the environment conducive to convective cloud formation. Some general circulation models (GCMs) do not include the methane hydrological cycle and some do. Those that do not (Hourdin et al. 1995; Mitchell et al. 2006; Tokano et al. [AU9] 1999; Richardson et al. 2007) always produce a single Hadley cell circulation, rising near the summer pole and with no causal relation to clouds at mid-latitudes. Those that do include the methane hydrological cycle (Rannou et al. 2006; Mitchell et al. 2006) have a terrestrial-like three-cell circulation. Haze aerosols could be important as cloud condensation nuclei (the contact parameter is not known) and so the transport of haze particles to locations in the troposphere could influence cloud formation. Figure 12.34 shows cloud predictions from the Rannou et al. (2006) GCM. Note the [AU10] relative maxima predicted cloud cover at both poles and near 35°S latitude. The circulation model of Mitchell et al. (2006) also predicted cloud formation at the poles and at latitude −40°, provided that the methane relative humidity is near 100%. The Rannou and Mitchell models make different predictions about the future occurrence of clouds at low latitudes. This is one possible observational test, although the relevant processes are numerous and complicated, weakening the potential value of this test. The latitudinal distribution of clouds appears to be changing with time as noted by Schaller

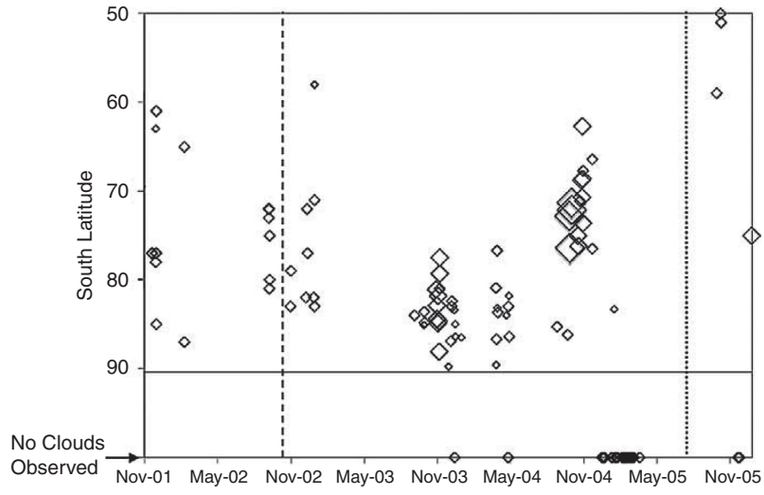

Fig. 12.33 From Schaller et al. (2006). Titan cloud locations vs time from ground-based observations. This figure excludes all mid-latitude clouds from Roe et al. (2005a) which are all located near 40°S and are clustered in longitude near 350°W. Diamond sizes indicate the relative size of the cloud observed. Dashed line marks Titan southern summer solstice which occurred in October 2002. Dotted line marks July 2005, the time at which the south pole ceased to be the area of maximum solar insolation on Titan. Before December 2004, clouds were observed within 30° of the south pole in nearly every adaptive optics image of Titan. During the 5 months period between December 2004 and April 2005 only one image shows even a small amount of cloud activity at the pole. Images taken in the 2005–2006 Titan apparition show a resurgence of Titan's clouds at the highest latitudes yet seen

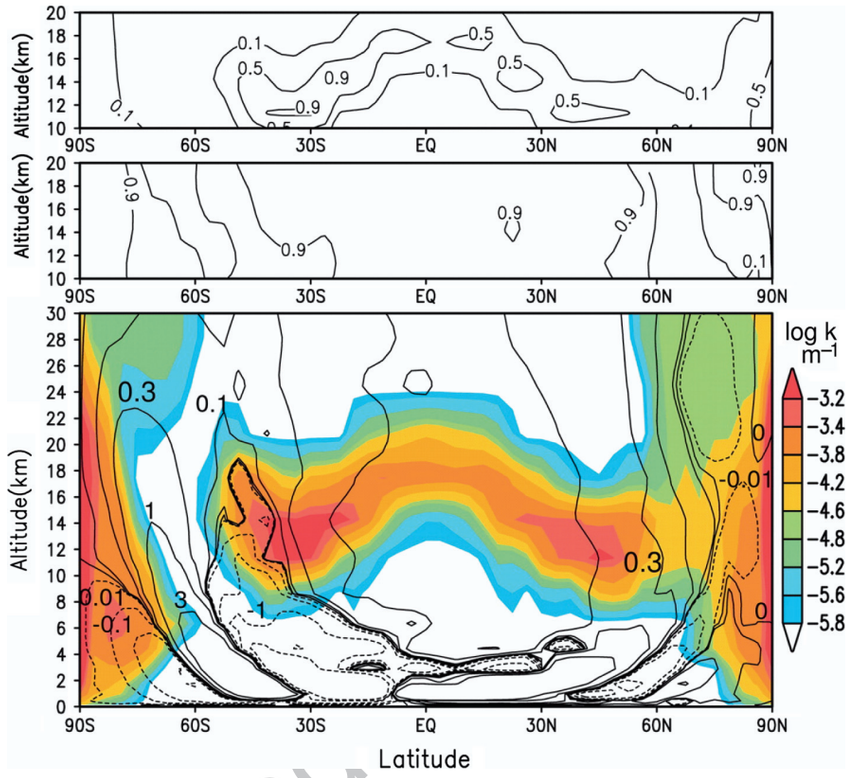

Fig. 12.34 From Rannou et al. (2006). Lower panel: modeled cloud extinction (m^{-1}) at 620 nm, averaged over one terrestrial year around the Cassini/Huygens arrival time, shown along with the stream function (10^9 kg s^{-1}) averaged over 7 years (one Titan season) before the Cassini arrival (*continuous lines denote clockwise motion*). Each result is actually the mean result of four consecutive Titan years. (*Middle panel*) The percentage of methane in drop composition (the remaining part is ethane). (*Top panel*) The fraction of time that cloud extinction exceeds a threshold of $k = 10^{-4}$ m^{-1}

et al. (2006) from ground-based observations (Fig. 12.33) and from recent Cassini ISS observations (Turtle et al. 2009) roughly in accord with model predictions, although some details such as the abrupt cessation of south polar clouds in late 2004 are not understood.

Highly ephemeral clouds form relatively frequently near latitude −40°. These are seen in ground-based images (Roe et al. 2005), in Cassini ISS images (Fig. 12.31 panels e–g) and Cassini VIMS images (Griffith et al 2005). The clouds form long, narrow streaks aligned in the east–west direction. This morphology would be consistent with venting from geyser or volcanic activity leading to cloud formation at an altitude where the vertical shear in zonal wind is strong, and this is the hypothesis favored by Roe et al. (2005). Griffith et al. (2005) favor a hypothesis which incorporates the large-scale circulation as discussed above. The longitudinal distribution seen in the accumulation of Cassini ISS images from 2004 to 2008 is broader than expected if the source were a single vent, and so disfavors the volcanic origin hypothesis (Turtle et al. 2009).

[AU11]

12.10.2 Stratospheric Condensates

At least three additional distinct types of condensate clouds are found in the north (winter) polar vortex (north of about 55° latitude). An ethane ice cloud covering a large aerial extent has been identified in the VIMS data (Griffith et al. 2006). Griffith et al. (2006) suggest that Titan's global circulation, with downwelling in the winter pole, brings photochemically-produced ethane from the stratosphere down to a cold winter troposphere where it forms an ice cloud.

Condensate signatures have also been observed in thermal-infrared spectra from both Voyager and Cassini. Several features in the Voyager Infrared Radiometer and Interferometer Spectrometer (IRIS) spectra could not be attributed to gaseous constituents. One of them (at 478 cm^{-1}) was identified by Khanna et al. (1987) as the ν_8 band of solid C_4N_2 (dicyanoacetylene; see also Samuelson et al. 1997). It is likely that this constituent and other condensates found only in the winter polar vortex region are produced as photochemical products from lower latitudes or higher altitudes, move into the shadow region either diffusively within the vortex or are advected from outside the vortex, and are not destroyed by sunlight once in the shadow region.

The Cassini CIRS (Composite Infrared Spectrometer) instrument provided additional data which constrain compositions of candidates which produce spectral features near 221 cm^{-1} and in the range 160–190 cm^{-1}. The feature centered at 221 cm^{-1} has not been identified. The other feature might be produced by HCN ice particles with radii less than about 5 μm (Samuelson et al. 2007). Samuelson et al. (2007) extended the work of Samuelson and Mayo (1991) and Mayo

and Samuelson (2005). De Kok et al. (2007) performed an analysis of the latitude and altitude distribution of the condensate spectral features. They identified four components. Two of them are widespread in latitude and are probably components of the global haze. One of these has a smaller scale height than the other. The other two components appear to be condensates based on their confined latitude and altitude distributions, reinforcing the results from Samuelson et al. (2007) and previous papers on condensates identified in thermal-infrared spectra.

Several inferences have been made regarding radii of stratospheric condensate cloud particles from far-IR spectra, using Mie theory coupled with a radiative transfer model. These results appear to be unique and suggest something about cloud growth and stability. These include particle radius determinations of: (1) 5–10 μm for C_4N_2 ice particles from the 478 cm^{-1} band (Samuelson et al. 1997), (2) 2–5 μm for a general ice cloud of unknown composition from continuum observations (Mayo and Samuelson 2005), (3) 2–5 μm for HCN ice particles from the 172 cm^{-1} band (Samuelson et al. 2007), and (4) about 2 μm for HC_3N ice particles from the 506 cm^{-1} band (Anderson et al. 2009). Anderson et al. (2009) also find evidence for ~6 μm C_4N_2 particles.

12.11 Prospects for Future Progress

To date, four types of observations have been used to study the aerosols in Titan's atmosphere. These include observations of the entire disk (one example is the geometric albedo spectrum) from the earth, observations of the spatially resolved disk from the earth using adaptive optics, observations from the Hubble Space Telescope (HST) of spectra or imaging at high spatial resolution, and observations from the Cassini/Huygens mission. Of these, only the observations from Huygens are complete and cannot be continued into the future. The observations by the Cassini orbiter by the Imaging Science System (ISS), by the Visible and Infrared Mapping Spectrometer (VIMS), and by the Composite Infrared Spectrometer (CIRS) will be continued for at least several years into the future. These observations will continue to increase our coverage over the disk of Titan. In addition, as time passes, we have the prospect of increasing the seasonal coverage of the aerosol distribution over the disk. This will materially add to our understanding of Titan's atmosphere. The spatially resolved observations from HST and from adaptive optics from the earth can also be continued to give more complete coverage of the seasonal changes on Titan.

At the current time we are just on the verge of beginning to see the results of coupled 2- and 3-dimensional models that include atmospheric circulation, aerosol production and heating, and chemistry. These theoretical studies are being increasingly constrained by the rich body of observations constraints including seasonal coverage.

At least two other sources of information are being accumulated that are sure to aid our understanding of the roles of aerosols in Titan's atmosphere. One includes the new laboratory studies of the optical constants of "tholin" material produced in laboratory simulations. Several new studies are underway covering the material produced under wider ranges of conditions including chemistry and energetics. A second source of new information includes improved absorption coefficients for methane under conditions of long paths and low temperatures that are closer to that found on Titan. This molecule has long been used to explore the vertical structure of Titan's aerosols. With new laboratory and theoretical studies, supplemented by the direct measurements in the near infrared on the Huygens probe, these approaches will be used with greater confidence to produce results with increasing accuracy.

Finally, we also have the prospect of additional new missions to Titan. Already studies of the possible new information that could be obtained by balloons, additional probes, and spacecraft in orbit around Titan are being explored. The rich environment of Titan will without doubt continue to be the subject of new studies on many fronts for years to come.

References [AU12]

Achterberg RK, Conrath BJ, Gierasch PJ, Flasar FM, Nixon CA (2008) Observation of a tilt of Titan's middle-atmospheric super-rotation. Icarus 197:549–555

Ádámkovics M, Wong MH, Laver C, de Pater I (2007) Widespread morning drizzle on Titan. Science 318:962–965

Anderson CM, Bjoraker G, Achterberg R (2007) Altitude distribution and wavenumber dependence of Titan's photochemical aerosol from Cassini/CIRS Observations. B.A.A.S. 39:530

Anderson CM, Samuelson RE, Bjoraker GL, Achterberg RK (2009) [AU13] Particle sizes and abundances of HC_3N and C_4N_2 ices in Titan's stratosphere at northern high latitudes. Submitted to Icarus

Bar-Nun A, Kleinfeld I, Ganor E (1988) Shape and optical properties of aerosols formed by photolysis of acetylene, ethylene, and hydrogen cyanide. J Geophys Res 93:8383–8387

Bar-Nun A, Dimitrov V, Tomasko M (2008) Titan's aerosols: comparison between our model and DISR findings. Planet Space Sci 56:708–714

Barth EL, Toon OB (2006) Methane, ethane, and mixed clouds in Titan's atmosphere. Properties derived from microphysical modeling. Icarus 182:230–250

Bernard J-M, Quirico E, Brissaud O, Montagnac G, Reynard B, McMillan P, Coll P, Nguyen M-J, Raulin F, Schmitt B (2006) Reflectance spectra and chemical structure of Titan's tholins: application to the analysis of Cassini–Huygens observations. Icarus 185:301–307

Brown ME, Bouchez AH, Griffith CA (2002) Direct detection of tropospheric clouds near Titan's south pole. Nature 420:795–797

Cabane M, Chassefiere E, Israel G (1992) Formation and growth of photochemical aerosols in Titan's atmosphere. Icarus 96:176–189

Cabane M, Rannou P, Chassefiere E, Israel G (1993) Fractal aggregates in Titan's atmosphere. Planet Space Sci 41:257–267

Coll P, Ramirez SI, Navarro-Gonzalez R, Raulin F (2001) Chemical and optical behaviour of tholins, laboratory analogues of Titan aerosols. Adv Space Res 27:289–297

Courtin R, Wagener R, McKay CP, Caldwell J, Fricke KH, Raulin F, Bruston P (1991) UVspectroscopy of Titan's atmosphere, planetary organic chemistry and prebiological synthesis. Icarus 90:43–56

Curtis DB, Hatch CD, Hasenkopf CA, Toon OB, Tolbert MA, McKay CP, Khare BN (2008) Laboratory studies of methane and ethane adsorption and nucleation onto organic particles: application to Titan's clouds. Icarus 195:792–801

de Kok R, Irwin PGJ, Teanby NA, Nixon CA, Jennings DE, Fletcher L, Howett C, Calcutt SB, Bowles NE, Flasar FM, Taylor FW (2007) Characteristics of Titan's stratospheric aerosols and condensate clouds from Cassini CIRS far-infrared spectra. Icarus 191:223–235

Fulchignoni M et al (2005) In situ measurements of the physical characteristics of Titan's environment. Nature 438:785–791

Griffith CA, Owen T, Miller GA, Geballe T (1998) Transient clouds in Titan's lower atmosphere. Nature 395:575–578

Griffith CA, Penteado P, Baines K, Drossart P, Barnes J, Bellucci G, Bibring J, Brown R, Buratti B, Capaccioni F, Cerroni P, Clark R, Combes M, Coradini A, Cruikshank D, Formisano V, Jaumann R, Langevin Y, Matson D, McCord T, Mennella V, Nelson R, Nicholson P, Sicardy B, Sotin C, Soderblom LA, Kursinski R (2005) The evolution of Titan's mid-latitude clouds. Science 310:474–477

Griffith CA, Penteado P, Rannou P, Brown R, Boudon V, Baines KH, Clark R, Drossart P, Buratti B, Nicholson P, McKay CP, Coustenis A, Negrao A, Jaumann R (2006) Evidence for a polar ethane cloud on Titan. Science 313:1620–1622

Hourdin F, Talagrand O, Sadourny R, Courtin R, Gautier D, McKay CP (1995) Numerical simulation of the general circulation of the atmosphere of Titan. Icarus 117:358–374

Hutzell WT, McKay CP, Toon OB, Hourdin F (1996) Simulations of Titan's brightness by a two dimensional haze model. Icarus 119: 112–129

[AU14] Imanaka H, Smith MA (2007a) Role of photoionization in the formation of complex organic molecules in Titan's upper atmosphere. Geophys Res Lett 34:L02204. doi:10.1029/2006GL028317

Imanaka H, Smith MA (2007b) Role of photoionization in the formation of complex organic molecules in Titan's upper atmosphere. Geophys Res Lett 34:L02204. doi:10.1029/2006GL028317

Imanaka H, Khare BN, Elsila JE, Bakes ELO, McKay CP, Cruikshank DP, Sugita S, Matsui T, Zare RN (2004) Laboratory experiments of Titaan tholin formed in cold plasma at various pressures: implications for nitrogen-containing polycyclis aromatic compounds in Titan haze. Icarus 168:344–366

Jennings DE, Flasar FM, Kunde VG, Samuelson RE, Pearl JC, Nixon CA, Carlson RC, Mamoutkine AA, Brasunas J, Guandique CE, Achterberg RK, Bjoraker GL, Romani PN, Segura ME, Albright SA, Elliott MH, Tingley JS, Calcutt S, Coustenis A, Courtin R (2009) Titan's surface brightness temperatures. Ap J Lett 691:L103–L105

Karkoschka E (1998) Methane, ammonia, and temperature measurements of the Jovian planets and Titan from CCD spectrophotometry. Icarus 133:134–146

Karkoschka E, Lorenz RD (1997) Latitudinal variation of aerosol sizes inferred from Titan's shadow. Icarus 125:369–379

Karkoschka E, Tomasko MG, Doose LR, See C, McFarlane EA, Schroder SE, Rizk B (2007) DISR imaging and geometry of the descent of the Huygens probe within Titan's atmosphere. Planet Space Sci 55:1896–1935

Khanna RK, Perera-Jarmer MA, Ospina MJ (1987) Vibrational infrared and Raman spectra of dicyanoacetylene. Spectrochim Acta 43A:421–425

Khare BN, Sagan C, Arakawa ET, Suits F, Calcott TA, Williams MW (1984) Optical constants of organic tholins produced in a simulated Titanian atmosphere: from X-ray to microwave frequencies. Icarus 60:127–137

Lavvas P, Yelle RV, Vuitton V (2008) The detached haze layer in Titan's atmosphere. Icarus in press [AU15]

Liang MC, Yung Y, Shemansky D (2007) Photolytically generated aerosols in the mesosphere and thermosphere of Titan. Astrophys J 661:L199–L202

Lockwood GW, Thompson DT (1979) A relationship between solar activity and planetary albedos. Nature 280:43–45

Lorenz RD, Smith PH, Lemmon MT, Karkoschka E, Lockwood GW, Caldwell J (1997) Titan's north-south asymmetry from HST and Voyager imaging: comparison with models and ground-based photometry. Icarus 127:173–189

Mayo LA, Samuelson RE (2005) Condensate clouds in Titan's north polar Stratosphere. Icarus 176:316–330

McGrath MA, Courtin R, Smith TE (1998) The ultraviolet albedo of Titan. Icarus 131:382–392

McGuigan M, Waite JH, Imanaka H, Sacks RD (2006) Analysis of Titan tholin pyrolysis products by comprehensive two-dimensional gas chromatography–time-of-flight mass spectrometry. J Chromatogr A 1132:280–288

McKay CP, Pollack JB, Courtin R (1989) The thermal structure of Titan's atmosphere. Icarus 80:23–53

Mitchell JL, Pierrelhumbert RT, Frierson DMW, Caballero R (2006) The dynamics behind Titan's methane clouds. Proc Nat Acad Sci USA 103:18421–18426

Nguyen M-J, Raulin F, Coll P, Derenne S, Szopa C, Cernogora G, Israël G, Bernard J-M (2008) From Titan's tholins to Titan's aerosols: Isotopic study and chemical evolution at Titan's surface. Adv Space Res 42:48–53

Penteado PF, Griffith CA, Tomasko MG, Engel S, See C, Doose L (2009) Latitudinal variations in Titan's methane and haze from Cassini VIMS observations. Icarus (submitted) [AU16]

Podolak M, Danielson RE (1977) Axel dust on Saturn and Titan. Icarus 30:479–492

Podolak M, Noy N, Bar-Nun A (1979) Photochemical aerosols in Titan's atmosphere. Icarus 40:193–198

Porco CC et al (2005) Imaging of Titan from the Cassini spacecraft. Nature 434:159–168

Rages K, Pollack JB (1983) Vertical distribution of scattering Hazes in Titan's upper atmosphere. Icarus 55:50–62

Rages K, Pollack JB, Smith PH (1983) Size estimates of Titan's aerosols based on Voyager high-phase-angle images. J Geophys Res 88, (NA11):8721–8728

Ramirez SI, Coll P, da Silva A, Navarro-González R, Lafait J, Raulin F (2002) Complex refractive index of Titan's aerosol analogues in the 200–900 nm domain. Icarus 256:515–529

Rannou P, Cabane M, Chassefoere E, Botet R, McKay CP, Courtin R (1995) Titan's geometric albedo: role of the fractal structure of the aerosols. Icarus 118:355–372

Rannou P, Cabane M, Botet R, Chassefiere E (1997) A new interpretation of scattered light measurements at Titan's limb. J Geophys Res 102:10977–11013

Rannou P, McKay CP, Lorenz RD (2003) A model of Titan's haze of fractal aerosols constrained by multiple observations. Planet Space Sci 51:963–976

Rannou P, Montmessin F, Hourdin F, Lebonnois F (2006) The latitudinal distribution of clouds on Titan. Science 311:201–205

Richardson MI, Toigo AD, Newman CE (2007) PlanetWRF: a general purpose, local to global numerical model for planetary atmospheric and climate dynamics. J Geophys Res 112:E09001

Rodin AV, Keller HU, Skorov YuV, Doose L, Tomasko MG (2009) Microphysical processes in Titan haze inferred from DISR/Huygens data. Icarus, (in press)

Roe HG, de Pater I, Macintosh BA, McKay CP (2002) Titan's clouds from Gemini and Keck adaptive optics imaging. Astrophys J 581: 1399–1406

Roe HG, Bouchez AH, Trujillo CA, Schaller EL, Brown ME (2005a) Discovery of temperate latitude clouds on Titan. Astrophys J 618: L49–L52

Roe HG, Brown ME, Schaller EL, Bouchez AH, Trujillo CA (2005b) Geographic control of Titan's mid-latitude clouds. Science 310:477–479

Roman MT, West RA, Banfield DJ, Gierasch PJ, Achterberg RK, Nixon CA, Thomas PC (2009) Determining a tilt in Titan's north–south albedo asymmetry from Cassini images. Icarus (in press)

Sagan C, Khare BN (1979) Tholins: organic chemistry of interstellar grains and gas. Nature 277:102–108

Sagan C, Thompson WR (1984) Production and condensation of organic gases in the atmosphere of Titan. Icarus 59:133–161

Samuelson RE, Mayo LA (1991) Thermal infrared properties of Titan's stratospheric aerosol. Icarus 91:207–219

Samuelson RE, Mayo LA, Knuckles MA, Khanna RJ (1997) C_4N_2 ice in Titan's north polar stratosphere. Planet Space Sci 45:941–948

Samuelson RE, Smith MD, Achterberg RK, Pearl JC (2007) Cassini CIRS update on stratospheric ices at Titan's winter pole. Icarus 189:63–71

Schaller EL, Brown ME, Roe HG, Bouchez AH, Trujillo CA (2006) Dissipation of Titan's south polar clouds. Icarus 184:517–523

[AU17] Shemansky D (2006) (needs title) in Abstracts of 36th COSPAR Scientific Assembly, 2006 July 16–23, Beijing, China (Paris: COSPAR), 2748

[AU18] Shemansky DE, Stewart AIF, West RA, Esposito LW, Hallett JT, Liu XM (2005a) The Cassini UVIS stellar probe of the Titan atmosphere. Science 308:978–982

Shemansky DE, Stewart AIF, West RA, Esposito LW, Hallett JT, Liu XM (2005b) The Cassini UVIS stellar probe of the Titan atmosphere. Science 308:978–982

Sicardy B., et al. (2006) The two Titan stellar occultations of 14 November 2003. J Geophys Res 111:E11S91, doi: 10.1029/2005JE002624

Signorell R, Jetzki M (2007) Phase behavior of methane haze. Phys Rev Lett . doi:10.1103/Phys Rev Lett.98.013401

Sromovsky LA, Suomi VE, Pollack JB, Krauss RJ, Limaye SS, Owen T, Revercomb HE, Sagan C (1981) Implications of Titan's north–south brightness asymmetry. Nature 292:698–702

Tokano T, Neubauer FM, Laube, McKay CP (1999) Seasonal variation of Titan's atmospheric structure simulated by a general circulation model. Planet Space Sci 47:493–520

Tomasko MG, Smith PH (1982) Photometry and polarimetry of Titan: pioneer 11 observations and their implications for aerosol properties. Icarus 51:65–95

Tomasko MG, Buchhauser D, Bushroe M, Dafoe LE, Doose LR, Eibl A, Fellows C, McFarlane E, Prout GM, Pringle MJ, Rizk B, See C, Smith PH, Tsetsenekos K (2002) The descent imager/spectral radiometer (DISR) experiment on the Huygens entry probe of Titan. Space Sci Rev 104:469–551

Tomasko MG, Archinal B, Becker T, Bezard B, Bushroe M, Combes M, Cook D, Coustenis A, de Bergh C, Dafoe LE, Doose L, Doute S, Eibl A, Engel S, Gliem F, Grieger B, Holso K, Howington-Kraus E, Karkoschka E, Keller HU, Kirk R, Kramm R, Kuppers M, Lanagan P, Lellouch E, Lemmon M, Lunine J, McFarlane E, Moores J, Prout GM, Rizk B, Rosiek M, Rueffer P, Schroder SE, Schmitt B, See C, Smith P, Soderblom L, Thomas N, West RA (2005) Rain, winds and haze during the Huygens probe's descent to Titan's surface. Nature 438:765–778

Tomasko MG, Bezard B, Doose L, Engel S, Karkoschka E (2008b) Measurements of methane absorption by the descent imager/spectral radiometer (DISR) during its descent through Titan's atmosphere. Planet Space Sci 56:624–647

Tomasko MG, Bezard B, Doose L, Engel S, Karkoschka E, Vinatier S (2008c). Heat balance in Titan's atmosphere. Planet Space Sci 56:648–659

Tomasko MG, Doose L, Engel S, Dafoe LE, West R, Lemmon M, Karkoschka E (2008c) A model of the aerosols in Titan's atmosphere. Planet Space Sci 56:669–707

Tomasko MG, Doose LR, Dafoe LE, See C (2009) Limits on the size of aerosols from measurements of linear polarization in Titan's atmosphere. Icarus (in press)

Toon OB, McKay CP, Courtin R, Ackerman TP (1988) Methane rain on Titan. Icarus 75:255–284

Toon OB, McKay CP, Griffith CA, Turco RP (1992) A physical model of Titan's aerosols. Icarus 95:24–53

Trafton LM (1973) Titan's spectrum and atmospheric composition. In Hunten DM (ed) The atmosphere of Titan. NASA SP-340, pp 17–41 [AU19]

Tran BN, Force M, Briggs RG, Ferris JP, Persans P, Chera JJ (2008) Titan's atmospheric chemistry: photolysis of gas mixtures containing hydrogen cyanide and carbon monoxide at 185 and 254 nm. Icarus 193:224–232

Turtle EP, Perry JE, McEwen AS, DelGenio AD, Barbara J, West RA, Fussner S, Dawson DD, Porco CC (2009) Cassini imaging of Titan's high-latitude lakes, clouds, and south-polar surface changes. Geophys Res Lett (in press)

Waite JH Jr, Young DT, Cravens TE, Coates AJ, Crary FJ, Magee B, Westlake J (2007) The process of tholin formation in Titan's upper atmosphere. Science 316:870–875

Walterscheid RL, Schubert G (2006) A vital explanation for Titan's haze layers. Icarus 183:471–478

West RA (1991) Optical properties of aggregate particles whose outer diameter is comparable to the wavelength. Appl Opt 30:5316–5324

West RA, Smith PH (1991) Evidence for aggregate particles in the atmosphere of Titan and Jupiter. Icarus 90:330–333

West RA, Lane AL, Hart H, Simmons KE, Hord CW, Coffeen DL, Esposito LW, Satao M, Pomphrey RB (1983) Voyager 2 photopolarimeter observations of Titan. J Geophys Res 88:8699–9708

West RA, Pitman KM, Martonchik JV, Dumont PJ (2008) Titan's stratospheric haze and its effect on surface contrast, Titan after Cassini–Huygens Book Symposium, Corpus Christi, TX, July 7–11

Wilson EH, Atreya SK (2003) Chemical sources of haze formation in Titan's atmosphere. Planet Space Sci 51:1017–1033

Young EF, Rannou P, McKay CP, Griffith CA, Noll K (2002) A three dimensional map of Titan's tropospheric haze distribution based on HST imaging. Astron J 123(6):3473–3486

Young DT et al (2004) Cassini plasma spectrometer investigation. Space Sci Rev 114:1–112

Yung YL, Allen M, Pinto JP (1984) Photochemistry of the atmosphere of Titan: comparison between model and observations. Astrophys J Suppl Ser 55:465–506

Author Queries:

AU1: Please specify Shemansky et al. 2005a or 2005b.
AU2: Lavvas et al. (2009) has been changed to Lavvas et al. (2008) as per the reference list. Please check.
AU3: Please provide text citation for Figure 12.9 and 12.10.
AU4: Brown et al., 2004 has been changed to Brown et al., 2002. Please check.
AU5: Lorenz et al. (1977) in the reference list.
AU6: Rodin (2009) has been changed to Rodin et al. (2009) as per the reference list. Please check.
AU7: Nieman et al. 2005 in the reference list.
AU8: Please specify Imanaka and Smith (2007a) or (2007b).
AU9: Tokano 1999 has been changed to Tokano et al. 1999 as per the reference list. Please check.
AU10: Rannou (2006) has been changed to Rannou et al. (2006). Please check.
AU11: Please specify Roe et al. 2005a or 2005b here and in other such occurrences.
AU12: Please provide text citation for the following references: Anderson et al. (2007), McGrath et al. (1998), and Young et al. (2002).
AU13: Please update submitted data.
AU14: Since there were two occurrences of Imanaka and Smith 2007, it has been changed to Imanaka and Smith 2007a and Imanaka and Smith 2007b. Also please check and change their respective text citations.
AU15: Please update in press details for the following references: Lavvas et al. 2008, Rodin et al. 2009, Roman et al. 2009, Tomasko et al. 2009, Turtle et al. 2009.
AU16: Please update submitted data.
AU17: Please update with title.
AU18: Since there were two occurrences of Shemansky et al. 2005, it has been changed to Shemansky et al. 2005a and Shemansky et al. 2005b. Also please check and change their respective text citations.
AU19: Please provide location.